



HAL
open science

Functional studies of CpSRP54 in diatoms show that the mechanism of thylakoid protein insertion differs from plants and green algae

Marianne Nymark, Marthe Caroline Grønbech Hafskjold, Charlotte Volpe, Davi de Miranda Fonseca, Animesh Sharma, Eirini Tsirvouli, Manuel Serif, Per Winge, Giovanni Finazzi, Atle Magnar Bones

► To cite this version:

Marianne Nymark, Marthe Caroline Grønbech Hafskjold, Charlotte Volpe, Davi de Miranda Fonseca, Animesh Sharma, et al.. Functional studies of CpSRP54 in diatoms show that the mechanism of thylakoid protein insertion differs from plants and green algae. *The Plant Journal*, 2021, 106 (1), pp.113-132. 10.1111/tpj.15149 . hal-03098197

HAL Id: hal-03098197

<https://hal.science/hal-03098197>

Submitted on 6 Jan 2021

HAL is a multi-disciplinary open access archive for the deposit and dissemination of scientific research documents, whether they are published or not. The documents may come from teaching and research institutions in France or abroad, or from public or private research centers.

L'archive ouverte pluridisciplinaire **HAL**, est destinée au dépôt et à la diffusion de documents scientifiques de niveau recherche, publiés ou non, émanant des établissements d'enseignement et de recherche français ou étrangers, des laboratoires publics ou privés.

1 **Functional studies of CpSRP54 in diatoms show that the mechanism of**
2 **thylakoid protein insertion differs from plants and green algae.**

3
4 Marianne Nymark^{#1}, Marthe Caroline Grønbech Hafskjold^{1,2}, Charlotte Volpe², Davi de
5 Miranda Fonseca^{3,4}, Animesh Sharma^{3,4}, Eirini Tsirvouli¹ Manuel Serif¹, Per Winge¹,
6 Giovanni Finazzi⁵, Atle Magnar Bones¹

7 ¹Department of Biology, Norwegian University of Science and Technology, N-7491,
8 Trondheim, Norway

9 ²Department of Biotechnology and Food Science, Norwegian University of Science and
10 Technology, N-7491, Trondheim, Norway

11 ³Department of Clinical and Molecular Medicine, Norwegian University of Science and
12 Technology, NTNU, N-7491 Trondheim, Norway

13 ⁴Proteomics and Modomics Experimental Core Facility (PROMEC), NTNU and Central
14 Administration, St Olavs Hospital, The University Hospital in Trondheim, Norway

15 ⁵Universit  Grenoble Alpes (UGA), Laboratoire de Physiologie Cellulaire et V g tale, UMR
16 5168, Centre National de la Recherche Scientifique (CNRS), Commissariat   l' nergie
17 Atomique et aux  nergies Alternatives (CEA), Institut National de la Recherche
18 Agronomique (INRA), Interdisciplinary Research Institute of Grenoble (IRIG), CEA-
19 Grenoble, 38000 Grenoble, France

20
21 **Running title: Effects of loss of CpSRP54 in diatoms**

25 Summary

26 The chloroplast signal recognition particle 54 kDa (CpSRP54) protein is a member of the
27 CpSRP pathway known to target proteins to thylakoid membranes in plants and green algae.
28 Loss of CpSRP54 in the marine diatom *Phaeodactylum tricornutum* lowers the accumulation
29 of a selection of chloroplast encoded subunits of photosynthetic complexes, indicating a role
30 in the co-translational part of the CpSRP pathway. In contrast to plants/green algae, absence of
31 CpSRP54 does not have a negative effect on the content of light-harvesting antenna complex
32 proteins and pigments in *P. tricornutum*, indicating that the diatom CpSRP54 protein has not
33 evolved to function in the post-translational part of the CpSRP pathway. *Cpsrp54* knockout
34 mutants display altered photophysiological responses, with a stronger induction of
35 photoprotective mechanisms and lower growth rates compared to wild type when exposed to
36 increased light intensities. Nonetheless, their phenotype is relatively mild, thanks to activation
37 of mechanisms alleviating the loss of CpSRP54, involving upregulation of chaperones. We
38 conclude that plants, green algae and diatoms have evolved differences in the pathways for co-
39 translational and post-translational insertion of proteins into the thylakoid membranes.

40

41 Introduction

42 Diatoms (Bacillariophyceae) are a species-rich group of unicellular, photosynthetic eukaryotes
43 found in freshwaters and oceans worldwide, which are of enormous ecological relevance
44 (Armbrust, 2009). This group of phytoplankton functions as a primary source of food for many
45 aquatic organisms and is responsible for performing similar levels of photosynthetic fixation
46 of carbon as all terrestrial rainforests combined (Nelson *et al.*, 1995, Armbrust, 2009, Gilbert
47 *et al.*, 2009). Diatoms are also promising organisms for a multitude of potential applications
48 within the bio-, nano- and environmental technologies (Bozarth *et al.*, 2009, Mishra *et al.*,
49 2017, Butler *et al.*, 2020). However, their role in primary production and potential for industrial
50 applications is not matched by the level of basic knowledge of their photosynthetic machinery.
51 Although the photosynthetic apparatus of Viridiplantae and Heterokonts such as diatoms share
52 many common features, they are separated from a common ancestor by more than a billion
53 years of evolution (Hohmann-Marriott and Blankenship, 2011). Diatoms arose by a secondary
54 endosymbiotic event and as a result their chloroplasts are surrounded by four membranes
55 (Gibbs, 1981, Flori *et al.*, 2016). Instead of having thylakoids organized into grana stacks
56 interconnected by stroma-exposed lamellae typical for land plants and green algae, diatom
57 thylakoids are organized in stacked bands of three thylakoids each, spanning along the entire

58 length of the plastid (Gibbs, 1970, Grouneva *et al.*, 2013). Photosystem II (PSII), cytochrome
59 b₆f (Cytb₆f), photosystem I (PSI) and ATP synthase are multi-subunit protein complexes
60 embedded in the thylakoid membranes and responsible for photosynthetic electron transport
61 and ATP synthesis together with protein-bound and mobile electron carriers (Nelson and Ben-
62 Shem, 2004). Light energy is collected and delivered to PSs by light harvesting complexes
63 (LHCs) consisting of pigments and pigment-binding proteins. While the pigment-binding
64 proteins of diatoms and plants/green algae belong to the LHC protein (LHCP) superfamily,
65 they bind different pigments (Grossman *et al.*, 1995, Dittami *et al.*, 2010). The LHCPs of the
66 green lineages (LHCa and LHCb) bind mainly Chl *a* and Chl *b*, whereas diatoms contain a
67 different subfamily of LHCPs that in addition to Chl *a* also bind Chl *c* and fucoxanthin (Fx)
68 and are therefore called Fx-Chl *a/c*-binding proteins (FCPs). The photosynthetic apparatus of
69 eukaryotic organisms is composed of proteins encoded by both nucleus and chloroplast
70 localized genes. In Viridiplantae, the nucleus encoded LHCPs and selected chloroplast encoded
71 proteins are guided to thylakoid membranes by the Chloroplast Signal Recognition Particle
72 (CpSRP) pathway (Kirst and Melis, 2014, Jeong *et al.*, 2017, Ziehe *et al.*, 2017, Ziehe *et al.*,
73 2018). The CpSRP54 GTPase of the CpSRP pathway has a dual function in plants and targets
74 proteins both post-translationally (LHCPs) and co-translationally (chloroplast-encoded
75 thylakoid membrane proteins) to thylakoids in cooperation with other members of the pathway
76 (Pilgrim *et al.*, 1998, Amin *et al.*, 1999, Rutschow *et al.*, 2008, Hristou *et al.*, 2019). In contrast
77 to the universally conserved SRP54 protein that plays an essential role in mediating co-
78 translational targeting of newly synthesized proteins to cellular membranes across all kingdoms
79 of life, the function of plant CpSRP54 is not dependent on an SRP RNA (Träger *et al.*, 2012,
80 Ziehe *et al.*, 2017). In the post-translational pathway of plants, CpSRP54 is part of the LHCP-
81 CpSRP43-CpSRP54-CpFTSY complex that guides LHCPs from the chloroplast membrane to
82 the thylakoid membrane, where the ALBINO3 (ALB3) insertase mediates protein insertion
83 (Ziehe *et al.*, 2018). In the co-translational pathway, CpSRP54 interacts with nascent
84 polypeptides and targets translating ribosomes to thylakoid membranes (Nilsson *et al.*, 1999,
85 Nilsson and van Wijk, 2002, Piskozub *et al.*, 2015, Hristou *et al.*, 2019). Differences in the
86 function of CpSRP54 have been reported between plants and green algae. The *Chlamydomonas*
87 *reinhardtii* CpSRP54 does not form a complex with the plastid specific chaperon CpSRP43
88 and is not involved in LHCP recognition, but is believed to function downstream of CpSRP43
89 together with its receptor CpFTSY in the posttranslational pathway (Dünschede *et al.*, 2015,
90 Jeong *et al.*, 2017). In both plants and green algae *cp srp54* knock out mutants, loss of CpSRP54
91 causes decreased levels of LHCPs and, consequently, lower pigment levels and paler green

92 coloration than in their wild type counterparts (Amin *et al.*, 1999, Rutschow *et al.*, 2008, Jeong
93 *et al.*, 2017, Hristou *et al.*, 2019). *Arabidopsis thaliana* CpSRP54 co-translationally associates
94 with a range of different subunits of the photosynthetic electron transport chain complexes, but
95 a similar function has not been reported in *C. reinhardtii* (Nilsson *et al.*, 1999, Nilsson and van
96 Wijk, 2002, Piskozub *et al.*, 2015, Jeong *et al.*, 2017, Hristou *et al.*, 2019). In diatoms,
97 homologues of CpSRP54, CpFTSY and two variants of ALB3 (ALB3a and ALB3b) have been
98 identified, whereas CpSRP43 homologues are absent (Träger *et al.*, 2012, Nymark *et al.*, 2019).
99 In addition, the LHCP translocation defect protein (LTD), which forwards LHCPs from the
100 chloroplast import machinery to the CpSRP complex in plants and green algae is apparently
101 also missing in diatom genomes (Ouyang *et al.*, 2011, Jeong *et al.*, 2018). A chloroplast
102 encoded SRP RNA is present in most, but not all diatom genomes sequenced to date (Träger
103 *et al.*, 2012, Brembu *et al.*, 2014). Information from gene models available at NCBI and The
104 Marine Microbial Eukaryote Meta/transcriptome Sequencing Project (MMETSP) database
105 reveal that the CpSRP54, CpFTSY and ALB3 proteins are widespread in all algae, including
106 red algae, haptophytes and the SAR (Stramenopila, Alveolata, and Rhizaria) clade. The LTD
107 and CpSRP43 related proteins are probably restricted to the green lineage, even though some
108 CpSRP43-like ankyrin-repeat proteins can be found in red algae, haptophytes, and in several
109 species within the SAR clade. The CpSRP43-like ankyrin-repeat proteins are missing in
110 Bolidophyceae and diatoms.

111

112 The function of ALB3b was recently investigated in the model diatom *Phaeodactylum*
113 *tricornutum*, where loss of the insertase caused a striking change in cell color from brown to
114 green (Nymark *et al.*, 2019). The change in pigmentation was caused by a ~75% decrease of
115 the main group of FCP proteins (LHCFs) and a subsequent lowered level of antenna pigments
116 (including fucoxanthin that provides the brown color of diatoms). The phenotype of the *alb3b*
117 mutants pointed to a role of this protein in posttranslational insertion of FCPs into the thylakoid
118 membrane. However, the ALB3b protein does not contain the basic Lys-rich C-terminal
119 domain (CTD) known from plants to interact with other members of the CpSRP pathway (Falk
120 *et al.*, 2010, Horn *et al.*, 2015, Chandrasekar and Shan, 2017). Instead, a CTD conserved within
121 the group of diatoms was identified in the ALB3b insertase, but its protein interaction partners
122 are unknown (Nymark *et al.*, 2019). ALB3a does contain the basic Lys-rich CTD, but repeated
123 attempts to create knock out mutants of this insertase were unsuccessful, implying a crucial
124 function in the co-translational CpSRP pathway similar to ALB3 and ALB3.2 of plants and
125 green algae, respectively (Sundberg *et al.*, 1997, Göhre *et al.*, 2006, Nymark *et al.*, 2019).

126 Previously published experiments with *P. tricornutum cpsrp54* mutants indicated that loss of
127 CpSRP54 causes increased high light sensitivity based on a more profound decrease in
128 photosynthetic efficiency in mutants compared to WT when exposed to high intensity blue
129 light (Nymark *et al.*, 2016). However, changes in the cell content of pigments and FCPs were
130 not tested in mutant lines. Knowledge of the roles of members of the diatom CpSRP pathway
131 is very limited, but based on currently available data CpSRP54 has been hypothesized to play
132 a part in the co-translational part of the CpSRP pathway, but not in the post-translational part
133 (Nymark *et al.*, 2016, Nymark *et al.*, 2019). To achieve further insight into the role of CpSRP54
134 in the CpSRP pathway, we investigated changes in photosynthetic properties, pigment level,
135 protein abundance and growth characteristics as a response to light stress in *P. tricornutum*
136 *cpsrp54* knockout (KO) lines. We propose a model illustrating the mechanistic differences of
137 thylakoid protein insertion in diatoms, plants and green algae.

138 Results

139 Structural features of diatom CpSR54 proteins

140 The diatom CpSRP54 protein harbors the conserved multidomain structure of SRP54 proteins:
141 A N-terminal helical bundle domain, a central SRP GTPase (G) domain and a methionine rich
142 M-domain (Figure 1A). The N and G domains form a functional unit called the NG domain
143 that is generally known to be necessary for binding and hydrolyzing GTP and interaction with
144 a similar NG domain in its receptor, the FTSY protein (Pool, 2005, Ziehe *et al.*, 2017). The M-
145 domain contains the conserved SRP RNA binding motif and is also responsible for interaction
146 with ribosomes and signal sequences of cargo proteins (Pool, 2005, Chandrasekar and Shan,
147 2017, Ziehe *et al.*, 2017, Hristou *et al.*, 2019). In addition, the CpSRP54 contains a chloroplast
148 targeting peptide (CTP). In plants, a conserved motif within the C-terminal region of the M-
149 domain, ARKKR, is known to be important for CpSRP43 binding (Funke *et al.*, 2005,
150 Dünschede *et al.*, 2015). This motif is poorly conserved in diatom CpSRP54 proteins and in
151 CpSRP54 from *C. reinhardtii* which does not bind CpSRP43 (Figure 1D) (Dünschede *et al.*,
152 2015). These proteins contain a polybasic motif with two conserved arginines (the RR-motif
153 in Figure 1A and D). The GTPase G1-G5 domains, the I-box, “ALL[DE]ADV”, “D[SA]RGG”,
154 and “RILGMGD” motifs are all present in diatom CpSRP54 proteins. However, CpSRP54
155 proteins in diatoms have a 24 – 26 amino acid insertion between the G1 and G2 domain (Figure
156 1B). A model based on the crystal structure of *Arabidopsis thaliana* CpSRP54 and FTSY (PDB
157 ID: 5L3R) using Swiss Model (Waterhouse *et al.*, 2018) suggests that this amino acid insert
158 forms a loop-structure that does not directly interfere with the CpSRP54-FTSY interaction

159 surface (Figure 1C).

160

161 CRISPR/Cas9 editing of *CpSRP54* resulted in frame-shift mutations

162 Three CRISPR/Cas9 derived *cpsrp54* mutant lines (*cpsrp54-8*, *cpsrp54-11*, *cpsrp54-20*)
163 originating from single cells from the M2, M4 and M8 lines, respectively (Nymark *et al.*, 2016)
164 were selected for functional characterization. Frame-shift mutations were confirmed in all cell
165 lines by TOPO cloning and subsequent Sanger sequencing of PCR products spanning the
166 region targeted by the Cas9-gRNA complex. The Cas9/gRNA complex was designed to target
167 a part of the *CpSRP54* gene (Phatr2_35185; XM_002179577) encoding the SRP54 N-terminal
168 helical bundle domain of the CpSRP54 protein (Figure 1A). Polymorphisms in the *CpSRP54*
169 gene confirmed that both alleles had been amplified and sequenced for *cpsrp54-8* and *cpsrp54-11*
170 (*11*) (Figure S1). Both *cpsrp54-8* and *cpsrp54-11* contained small indels. *Cpsrp54-20* contained
171 a 212 bp insertion in one allele consisting of fragments from one of the vectors used for
172 transformation of the *P. tricornutum* cells (Figure S1). The other allele of the *cpsrp54-20* line
173 could not be amplified indicating larger insertions or deletion events preventing amplification
174 by PCR. The frame-shift mutations caused premature stop codons shortly after the indels,
175 resulting in truncated CpSRP54 proteins (Figure 1E).

176

177 *Cpsrp54* mutants showed no visible coloration phenotype

178 The *alb3b* mutants displayed a distinct difference in coloration, lower absorbance in the blue-
179 green part of the spectrum and a decreased transfer of energy from light harvesting antenna
180 pigments Fx and Chl *c* to PSII compared to WT (Nymark *et al.*, 2019). If CpSRP54 functions
181 in the same part of the CpSRP pathway as ALB3b, a similar phenotype would be expected.
182 Cell culture color, *in vivo* fluorescence excitation and absorbance spectra from *cpsrp54* mutants
183 and WT were therefore recorded. No visible color change could be seen in *P. tricornutum*
184 *cpsrp54* mutants compared to WT that would indicate major differences in light harvesting
185 antenna pigments content (Figure 2A). This observation was further supported by the close to
186 identical *in vivo* fluorescence excitation and absorbance spectra from mutants and WT (Figure
187 2B-C). These results imply that the ability of mutants and WT to harvest light energy for
188 photosynthesis as well as the different pigment's relative energy transfer efficiency to Chl *a* in
189 the reaction center of PSII are identical (Figure 2B). The presented results are all from low
190 light (LL, 35 $\mu\text{mol photons m}^{-2} \text{s}^{-1}$) acclimated cells.

191

192 *Cpsrp54* mutants are sensitive to increased light intensities

193 Based on the lack of a visible phenotype in LL and the indication that the *cpsrp54* mutants
194 might be sensitive to increased light intensities (Nymark *et al.*, 2016), we decided to perform
195 a more thorough investigation of pigment content and photophysiological responses of the
196 *cpsrp54* mutants by exposing LL-acclimated cells (0 h) to medium light (ML, 200 μmol
197 $\text{photons m}^{-2} \text{s}^{-1}$) intensities for 0.5, 6, 24, 48, and 168 h. Additionally, we calculated the
198 stoichiometry of functional reaction centers, the photosynthetic electron flow and growth rates
199 in LL and ML acclimated cells. As expected from the close to identical color and *in vivo*
200 fluorescence excitation spectra, the pigment analyses confirmed that the content of Chl *a* and
201 Fx in *cpsrp54* lines was similar to WT at most time points during the time series study (Figure
202 3A-B). In contrast, the conversion of the xanthophyll cycle pigment diadinoxanthin (Ddx) to
203 the photoprotective pigment diatoxanthin (Dtx) was greatly enhanced in the mutants after the
204 shift from LL to ML conditions as illustrated by the significantly higher Dtx content per cell
205 (Figure 3D) and the elevated de-epoxidation state index (DES; $\text{DES} = \text{Dtx}/(\text{Dtx}+\text{Ddx})$; Figure
206 3E). Whereas the conversion of Ddx to Dtx peaked at the 0.5 h time point in the WT samples,
207 the DES index reached its maximum after 6 h in ML in the *cpsrp54* lines and stayed at a higher
208 level than WT during the entire length of the ML exposure experiment. In addition, the non-
209 photochemical quenching (NPQ) capacity of the mutants was found to be 20-30% higher than
210 that of the WT samples (Figure 3F). Altogether, these responses point towards a higher level
211 of light stress in the mutants compared to the WT.

212 Chl *a* variable fluorescence measured with a pulse-amplitude modulated (PAM) fluorometer
213 was used to monitor the physiological response of LL-acclimated *cpsrp54* KO mutants during
214 acclimation to ML intensity. The photosynthetic (PSII) efficiency (F_v/F_m), the maximum light-
215 utilization coefficient (the slope of the photosynthesis versus irradiance curves; α), the
216 photosynthetic capacity (maximum relative electron transport rate, $r\text{ETR}_{\text{max}}$) and the light
217 saturation index ($E_k = r\text{ETR}_{\text{max}}/\alpha$) were similar in *cpsrp54* and WT cultures in LL-acclimated
218 cells (Figure 4A-D). Exposure to ML caused only a minor drop in F_v/F_m in WT cultures,
219 whereas F_v/F_m was significantly lower in *cpsrp54* cultures compared to WT at all time points
220 after the shift from LL to ML (Figure 4A). These results imply increased levels of photodamage
221 and/or photoprotection when CpSRP54 is absent. The WT cells showed the expected response
222 to increased light intensities displaying a pronounced increase in $r\text{ETR}_{\text{max}}$ and E_k as a function
223 of ML exposure time. In contrast, these values decreased or remained at LL levels in the
224 *cpsrp54* cultures. The functional status of the photosynthetic apparatus of the *cpsrp54* mutants
225 was compared to that of WT cells using the ElectroChromic Shift (ECS) signal. This is the

226 stark effect, i.e. a modification of the absorption properties of membrane embedded
227 photosynthetic pigments following the buildup of a trans-thylakoid membrane potential during
228 photosynthesis (Witt, 1979). The ECS signal can be used to determine spectroscopically the
229 stoichiometry of functional reaction centers and the photosynthetic electron flow (Bailleul *et*
230 *al.*, 2010). We used this approach to compare LL and ML-acclimated cells and found that the
231 fraction of functional PSII reaction centers (RC) per functional PSI RC were less than half in
232 the mutants compared to the WT in ML-acclimated cells, whereas no significant differences
233 were found in LL-acclimated cells (Figure 4E). Similarly, the photosynthetic electron flow was
234 around 50% lower in ML-grown *cpsrp54* lines than in WT cells (Figure 4F). The decreased
235 photophysiological fitness of the *cpsrp54* mutants in ML is reflected also in an approx. 20%
236 slower growth rate compared to WT at this light intensity (Table 1). The difference in growth
237 rate did not increase further when the cells were grown in high light (HL; 1000 $\mu\text{mol photons}$
238 $\text{m}^{-2} \text{s}^{-1}$).

239

240 [Decreased rate of PSII repair](#)

241 The increased susceptibility of the *cpsrp54* mutants to ML demonstrated above indicates an
242 enhanced photosensitivity of the mutant strains, which could result from either an increased
243 rate of photodamage to PSII core proteins or a decreased rate of PSII repair. To separate
244 between these two phenomena, we performed an experiment where lincomycin (LINC), an
245 inhibitor of chloroplast translation, was added to LL-acclimated cells before exposure to high
246 light (HL; 1000 $\mu\text{mol photons m}^{-2} \text{s}^{-1}$) for 1 h. In parallel, cells without LINC were exposed to
247 the same light treatment. Addition of LINC removes the possibility to synthesize new
248 chloroplast proteins and PSII repair cannot take place. F_v/F_m was measured before the HL-
249 treatment, after 1 h of HL, and after 30 min of recovery after the HL-treatment as an indicator
250 of PSII functionality. The measurements performed directly after the 1 h HL treatment will be
251 affected both by thermal dissipation of absorbed light energy (qE) and photodamaged PSII
252 reaction centers (qI). 30 min of recovery in very dim light allows for relaxation of the rapidly
253 reversible qE component of NPQ. No significant differences were found between LL-
254 acclimated cultures or between cultures exposed to HL after addition of LINC (Figure 5). The
255 HL+LINC combination caused a severe and close to identical decrease in F_v/F_m in WT and
256 *cpsrp54* lines. An increase in F_v/F_m from ~25% to ~39 % of LL-levels was detected at the end
257 of the 30 min dark period which can probably be attributed to relaxation of qE, although LINC
258 might slow down the process (Bachmann *et al.*, 2004). Significant differences were found

259 between WT and *cpsrp54* lines in HL-treated cells without the addition of LINC (two-tailed
260 Student's t-tests ($p < 0.05$); Figure 5). After relaxation of qE, F_v/F_m recovered to 90% of the LL-
261 levels in WT, whereas the equivalent average value in the *cpsrp54* cultures was ca. 70%. It is
262 important to be aware that the use of the F_v/F_m to assess photodamage is liable to artefacts.
263 Upon strong illumination, long living fluorescence quenching phenomena other than
264 photodamage can contribute to change in fluorescence yield (Dall'Osto *et al.*, 2005). However,
265 the fact that F_v/F_m recovers comparably in WT and mutants after LINC treatment (i.e. blocking
266 PSII repair cycle; Figure 5) suggests that, if other long living quenching processes than
267 photoinhibition were induced in our conditions, they were of the same extent in both genotypes.
268 Our combined results are therefore interpreted to indicate that the rate of PSII repair is
269 negatively affected by absence of CpSRP54, whereas the rate of PSII inactivation is highly
270 similar.

271 Differences at the protein level

272 To investigate the effect of loss of CpSRP54 on the level of chloroplast proteins, quantitative
273 proteomics of *cpsrp54-8* and *cpsrp54-11* cells that had been exposed to ML for 6 h was
274 performed and compared to WT samples. The 6 h time point was chosen since the pigment and
275 variable Chl fluorescence measurements described above indicated a high level of light stress
276 at this timepoint in *cpsrp54* lines. Only proteins encoded in the chloroplast genome or predicted
277 to contain chloroplast transit peptides sequences were chosen for analysis. Chloroplast proteins
278 that were significantly regulated (FDR < 0.01) in the same direction in both *cpsrp54* lines,
279 showing \log_2 ratios $\geq \pm 0.5$ for at least one of the mutant lines and where at least two unique
280 peptides were detected are included in Table 2. We further investigated the relative protein
281 expression level of selected proteins by western blot. The most interesting findings are listed
282 below.

283

284 Effects on the photosynthetic apparatus

285 Several FCPs involved in light harvesting were moderately affected in the *cpsrp54* mutant lines
286 after 6 h of ML exposure, but the regulation was in most cases found to go in opposite direction
287 in *cpsrp54-8* and *cpsrp54-11* compared to WT, meaning that none of these FCP proteins
288 fulfilled the criteria for being included in Table 2. The significantly, but moderately, regulated
289 FCP proteins were in general expressed at a lower level than WT in *cpsrp54-8* and at a higher
290 level in *cpsrp54-11* (Supplementary Dataset 1). After 6 h in ML, the diatoms will be in the

291 process of downsizing their light harvesting antenna, and the results might reflect differences
292 in acclimation status. Since the proteomics data recorded for the FCPs was inconclusive with
293 regards to the effect of absence of CpSRP54, western blot analyses were additionally
294 performed for a subgroup of FCPs, the LHCFs. The LHCF subgroup contains the major light-
295 harvesting proteins in diatoms. The expression level of these proteins was investigated in total
296 protein extracts from LL-acclimated cells, cells exposed to 6 h ML and ML-acclimated cells
297 using an antibody predicted to detect LHCF1-11 (Figure 6A) (Juhas *et al.*, 2014). The observed
298 differences in LHCF expression levels were very modest between mutants and WT, and
299 additional blots were therefore produced from total protein extracts from LL and ML-
300 acclimated cells. Relative abundances of LHCF proteins were estimated based on average
301 ratios between *cpsrp54* and WT lines from several blots and two independent experiments
302 (Figure S2). No differences in LHCF content was found between *crpsrp54* lines and WT in
303 LL-acclimated cells, whereas prolonged growth in ML seemed to induce somewhat higher
304 expression of LHCF proteins in the mutants than in WT (Figure 6B). These results are in line
305 with the spectral properties (Figure 2) and light harvesting pigment data (Figure 3A-B)
306 described above, indicating that loss of CpSRP54 does not result in a smaller light harvesting
307 antenna in the *cpsrp54* lines.

308 Eleven chloroplast-encoded and one nucleus-encoded subunit of the photosynthetic electron
309 transport (PET) chain complexes PSII, PSI, Cytb₆f and ATPase fulfilled the above described
310 criteria and were found to be moderately downregulated in the *cpsrp54* lines compared to WT
311 after exposure to 6 h of ML (Table 2). Prolonged exposure to ML caused a decrease of the ratio
312 of functional PSII/PSI in *cpsrp54* lines (Figure 4E). Light induced inactivation of PSII is
313 typically caused by damage to the PSII RC core protein D1 (PsbA), but the proteomics data
314 indicated that the lack of CpSRP54 had the strongest negative effect on the other PSII RC core
315 protein D2 (PsbD; Table 2). D2 was among the strongest downregulated PET chain subunits,
316 whereas D1 was only significantly downregulated in one of the mutant lines (Supplementary
317 Dataset 1). To get a better overview of the content of PSII RC proteins in *cpsrp54* lines relative
318 to WT, western blot analyses was performed on total protein extracts from LL-acclimated cells,
319 cells exposed to 6 h ML and ML acclimated cells with antibodies specific to D1 and D2. The
320 initial analysis of D1 and D2 supported a generally lower amount of D2 in the mutants
321 compared to WT, whereas no clear effect on the relative abundance of D1 was observed at any
322 light treatment (Figure 6A). As for the LHCF proteins relative quantification of D1 and D2
323 levels in LL and ML was performed running additional western blots (Figures S3-S4). Average

324 relative abundance values for D1 and D2 are presented in Figure 6C-D. The results indicated
325 that D2 protein levels in *cpsrp54* mutants were lowered to around 70% of WT levels in both
326 LL and ML conditions (Figure 6D). The relative content of D1 in mutants compared to WT
327 showed larger variation between experiments, but was close to WT levels on average (Figure
328 6C; Figure S3). A negative effect of loss of CpSRP54 on the amount of D1 could therefore
329 neither be proven from the proteomics nor the western blot analyses. In contrast to PSII core
330 proteins, the subunits comprising the oxygen evolving complex (OEC) of PSII are mainly
331 nucleus-encoded (except for PsbV). Of the OEC proteins detected by the proteomics data,
332 PSBO, OEE3 and PsbV were unaffected by the loss of CpSRP54, whereas PSBP was slightly
333 upregulated (Table 2). As for the PSII RC protein D1, the PSI RC proteins PsaA and PsaB were
334 also only significantly downregulated in one of the lines, but the abundance of five other
335 chloroplast-encoded PSI core subunits was found at lower levels in both mutant lines than in
336 WT (Table 2; Supplementary Dataset 1). Two ferredoxin NAPD(H) reductases (FNRs), both
337 nuclear-encoded, were among the strongest upregulated proteins in the dataset. FNR mainly
338 catalyzes the final step in linear electron transport, reducing NAPD^+ to NADPH, but in plants
339 some isoforms might also be involved in cyclic electron flow (CEF) around PSI, resulting in
340 ATP formation (Goss and Hanke, 2014). However, the contribution of CEF in ATP production
341 in diatoms is negligible (Bailleul *et al.*, 2015). The increased amount of FNR in *cpsrp54*
342 mutants might be an attempt to compensate for the lower amounts of electrons available for
343 NADPH formation in the mutants (Figure 4C and 4F).

344 [Up-regulation of proteins connected to photoprotective responses](#)

345 Several proteins known or predicted to be involved in photoprotective mechanisms were
346 detected at moderately higher levels in mutants compared to WT (Table 2). LHCX1 and
347 LHCX2 are FCP proteins important for NPQ and were upregulated in *cpsrp54* lines, consistent
348 with the NPQ phenotype of the mutants (Figure 3F). A putative thylakoid bound ascorbate
349 peroxidase (APX) likely to be involved in removal of H_2O_2 produced during photosynthesis
350 was also expressed at higher levels in the mutants than in the WT. In addition, the expression
351 of a protein annotated as a Cyclophilin type peptidyl-prolyl cis-trans isomerase was increased
352 by around 50% in the mutants (Table 2). Chloroplast-localized cyclophilin type proteins has
353 been found to be important for PSII biogenesis and repair in plants (Fu *et al.*, 2007, Järvi *et al.*,
354 2015).

355 [Up-regulation of chaperones and possible interaction partners](#)

356 Chloroplast-localized members of the four major families of ATP-dependent molecular

357 chaperones (chaperonin/Cpn60, Hsp70, Hsp90 and Hsp100 families) and cofactors were
358 detected by the proteomics analyses. Of these, the chloroplast chaperon annotated as DnaK
359 (Hsp70, chloroplast genome), its co-chaperone DNAJ (Hsp40) and the Hsp100 chaperone
360 CLPB were expressed at higher levels in both the investigated mutant lines than in WT, with
361 DnaK being the most upregulated chloroplast protein in our dataset (Table 2). The functions of
362 these chaperons are unknown in diatoms, but HSP70 (DnaK homologs)- and HSP40 (DNAJ
363 homologs)-type chaperons are known to be part of a network of molecular chaperons important
364 for co-translational folding in chloroplasts (Ries *et al.*, 2020). In addition to protein folding,
365 other proposed functions of stromal HSP70 chaperones include protein import into
366 chloroplasts, protection/repair of PSII from photoinhibition and (dis-) assembly of vesicle-
367 inducing protein in plastids 1 (VIPP1) oligomers (Trösch *et al.*, 2015). VIPP1 (also called the
368 inner membrane-associated protein of 30 kDa (IM30)) proteins are highly conserved proteins
369 found in cyanobacteria, algae and plants (Heidrich *et al.*, 2017, Siebenaller *et al.*, 2019). The
370 exact function of VIPP1 is unclear, but it is proposed to be multifunctional and to be involved
371 in thylakoid biogenesis/stabilization, coping with chloroplast membrane stress, remodeling of
372 thylakoid membranes during light shifts and co-translational insertions of photosynthetic
373 proteins (Walter *et al.*, 2015a, Heidrich *et al.*, 2017, Junglas and Schneider, 2018, Siebenaller
374 *et al.*, 2019). The *P. tricornutum* homolog of VIPP1 was upregulated almost 2-fold in the
375 *cpsrp54* mutants (Table 2). VIPP1 is known to dynamically shift between monomeric and
376 oligomeric states, likely with the help of chaperons (Siebenaller *et al.*, 2019). DnaK-type
377 chaperons and co-chaperones of the DNAJ type have been shown to interact with and impact
378 the oligomeric state of VIPP1 in other photosynthetic organisms (Liu *et al.*, 2007, Gao *et al.*,
379 2015, Siebenaller *et al.*, 2019). CLPB belongs to the family of Caseinolytic proteases (CLP)
380 that are important for removal of stress-related protein aggregates (Mishra and Grover, 2016).
381 CLPB-type chaperones have been found to collaborate and directly interact with the DnaK
382 system to solubilize and rescue aggregated proteins (Doyle *et al.*, 2015, Mogk *et al.*, 2015,
383 Mishra and Grover, 2016).

384

385 Discussion

386 CpSRP54 is unlikely to play a role in post-translational targeting of FCPs to thylakoid
387 membranes in diatoms

388 The role of CpSRP54 in the CpSRP pathway has previously been studied in the plant and green algal
389 model organisms *A. thaliana* and *C. reinhardtii*, respectively (Amin *et al.*, 1999, Nilsson *et al.*, 1999,
390 Hutin *et al.*, 2002, Nilsson and van Wijk, 2002, Rutschow *et al.*, 2008, Dünschede *et al.*, 2015, Walter
391 *et al.*, 2015b, Jeong *et al.*, 2017, Hristou *et al.*, 2019). CpSRP54 targets members of the LHCP family
392 to thylakoid membranes in both species through the post-translational pathway, and CpSRP54 KO
393 mutants display a pale green color as a result of having a truncated light harvesting antenna (TLA)
394 (Amin *et al.*, 1999, Hutin *et al.*, 2002, Rutschow *et al.*, 2008, Jeong *et al.*, 2017). In addition to the
395 color change and the lower levels of antenna proteins and pigments, typical features of TLA mutants
396 are increased photosynthetic activity per Chl and a higher light saturation point of photosynthesis
397 (Kirst *et al.*, 2012a, Kirst *et al.*, 2012b, Kirst *et al.*, 2014, Jeong *et al.*, 2017). These features were all
398 present in *P. tricornutum alb3b* mutants, and the TLA phenotype was interpreted as the ALB3b
399 insertase playing an important, but not essential role in integration of FCPs into the thylakoid
400 membrane in diatoms (Nymark *et al.*, 2019). In contrast, the *P. tricornutum cpsrp54* mutants did not
401 display any of the above described TLA-features, and they displayed the WT phenotype for almost
402 all measured parameters when grown in LL conditions. Taking into consideration also the CTD of
403 the ALB3b insertase having unknown interaction partners and the absence of key players of the LHCP
404 targeting machinery like the CpSRP43 chaperon and the LTD protein, an essential role for the diatom
405 CpSRP54 in post-translational targeting of FCPs to thylakoid membranes seems highly unlikely. The
406 post-translational part of the CpSRP pathway known to function in plants and green algae is the only
407 SRP-mediated protein targeting process that is not a co-translational process (Pool, 2005, Ries *et al.*,
408 2020). It is tempting to speculate that the diatom CpSRP54 protein has not evolved to function post-
409 translationally, and that an alternative strategy for targeting of FCPs to thylakoids exists in diatoms.
410 However, a study performed by Lang and Kroth two decades ago showed that FCP integration into
411 diatom thylakoid membranes is GTP-dependent (Lang and Kroth, 2001). They also showed that
412 LHCPs from peas could be inserted into diatom thylakoids in the presences of GTP and diatom
413 stromal extracts, and that diatom FCPs could be inserted into pea thylakoids under reciprocal
414 experimental conditions, although to a lesser extent. In both experiments a low fraction of
415 LHCPs/FCPs were seemingly also spontaneously integrated into thylakoids (Lang and Kroth, 2001).

416 At the time, the results were interpreted as LHCPs of plants and FCPs of diatoms being integrated
417 through a highly similar CpSRP-dependent machinery. In light of the current knowledge of the
418 CpSRP pathway in diatoms, another possible explanation for their results could be that the LHCPs
419 and FCPs are similar enough to be recognized by two different thylakoid protein targeting
420 machineries.

421

422 The phenotype of *cpsrp54* mutants indicates a role for the diatom CpSRP54 in the co-
423 translational CpSRP pathway

424 Phenotypic differences are triggered by increased light intensities

425 One of the aims of this study was to test the hypothesis of CpSRP54 being involved in co-translational
426 insertions of chloroplast encoded proteins into the thylakoid membrane. A shift from LL to ML
427 conditions resulted in photophysiological differences between *cpsrp54* and WT that were in support
428 of such a role. Despite stronger induction of photoprotective mechanisms (Figure 3D-F, Table 2)
429 physiological parameters indicated higher levels of PSII inactivation in *cpsrp54* mutants compared to
430 WT (Figure 4), likely to be caused by a moderately decreased rate of PSII repair (Figure 5). Similarly,
431 a moderately reduced PSII repair efficiency has also been reported for *A. thaliana* mutants lacking
432 CpSRP54 (Walter *et al.*, 2015b). Increased light intensities demand a higher rate of PSII repair
433 involving an efficient removal and replacement of chloroplast encoded proteins prone to
434 photodamage by a newly synthesized copy (Järvi *et al.*, 2015, Theis and Schroda, 2016). Loss of
435 CpSRP54 might cause the replacement of damaged PSII core proteins to be less efficient. In plants,
436 a connection between accumulation of non-functional PSII and down regulation of the activity and
437 amount of zeaxanthin epoxidase (ZEP) has been shown (Bethmann *et al.*, 2019). ZEP is responsible
438 for the reconversion of zeaxanthin to violaxanthin in plants and Ddx to Dtx in diatoms when the
439 photosynthetic electron transport is no longer saturated either because of acclimation of the
440 photosynthetic apparatus to higher light intensities or by transfer to low light conditions. If a
441 connection between decreased ZEP amount/activity and increased PSII inhibition exists also in
442 diatoms, it could explain the more limited back conversion of Dtx to Ddx in *cpsrp54* mutants after
443 prolonged ML-treatment. NADPH is a cofactor of ZEP, and a slower epoxidation of Dtx to Ddx
444 during acclimation to ML might also be caused by insufficient availability of NADPH because of the
445 lower electron flow rate in the *cpsrp54* lines (Lavaud and Goss, 2014).

446 Physiological differences cannot be explained by changes in the abundance of PSII RC proteins
447 Analyses of the proteome after 6 h of ML exposure were performed hoping that this data could
448 provide a molecular explanation for the light-induced phenotypic differences seen at the physiological
449 level. A straightforward explanation for the increased level of photoinactivated PSII in *cpsrp54* lines
450 would have been a decrease in the level of PSII RC proteins as a response to the light-treatment.
451 Photosynthetic organisms typically display a high turnover rate of D1, and to a lesser extent D2, when
452 subjected to increased light intensities (Aro *et al.*, 1993, Jansen *et al.*, 1996, Aro *et al.*, 2005, Rokka
453 *et al.*, 2005). In contrast, marine diatom species are shown to have more similar turnover rates for D1
454 and D2 (Wu *et al.*, 2011, Wu *et al.*, 2012). The proteomics data confirmed a lower relative abundance
455 of D2 in both the investigated *cpsrp54* lines, whereas the data for D1 was inconclusive. Additional
456 analysis of D1 and D2 in cells acclimated to LL and ML detected roughly 30% lower levels of D2 in
457 *cpsrp54* lines than in WT in both light conditions, whereas the relative amount of D1 varied between
458 experiments, but was on average more similar to WT levels. The consistently lower amount of D2
459 found in all light treatments therefore seems to be a general feature of the *cpsrp54* mutants, and not a
460 result of light stress. The photosynthetic performance of *cpsrp54* mutants is similar to WT levels in
461 LL, meaning that there is no difference in functionality of the assembled PSII complexes in the
462 mutants and WT, although the relative amount of one of the PSII core subunits seem to be lower. The
463 existence of sub-pools of D1 and D2 that were not a part of active PSII has previously been reported
464 for marine diatoms by Wu and coworkers (Wu *et al.*, 2011, Wu *et al.*, 2012). They also showed that
465 a decrease in PSII activity often did not correlate with changes in D1 and D2 abundance (Wu *et al.*,
466 2012). A similar phenomenon seems likely in our study since the relative lower content of D2
467 compared to WT under the same light conditions is stable, whereas the difference in photosynthetic
468 performance increases when shifted from LL to ML intensities. In support of our observations and
469 previous reports is also a recent study of PSII supercomplexes in *P. tricornutum* thylakoid
470 membranes, where a subpopulation of inactive/damaged PSII RCs not associated with FCP
471 complexes was observed and suggested to function as PSII repair stations (Levitan *et al.*, 2019). The
472 analysis of PSII RC proteins levels carried out in this study were performed on whole cell extracts
473 and will not separate between proteins incorporated in functional PSII, proteins in inactivated PSII
474 or unassembled D1 and D2 proteins.
475

476 Loss of *cpsrp54* triggers similar responses on the protein level in diatom and plants
477 In *A. thaliana*, there is convincing data supporting that CpSRP54 enhances the efficiency of co-
478 translational insertion of a selection of chloroplast encoded subunits (Amin *et al.*, 1999, Nilsson *et*
479 *al.*, 1999, Nilsson and van Wijk, 2002, Rutschow *et al.*, 2008, Piskozub *et al.*, 2015, Hristou *et al.*,
480 2019). Several studies have shown a reduced content of PSI and PSII RC proteins in developing *A.*
481 *thaliana cpsrp54* mutants (Amin *et al.*, 1999, Rutschow *et al.*, 2008, Hristou *et al.*, 2019), and
482 additional potential targets for CpSRP54 were revealed through a proteomic study, indicating that
483 also other subunits of PSI, PSII and ATP synthase were negatively affected by a lack of CpSRP54
484 (Rutschow *et al.*, 2008). Direct evidence for the interaction of nascent chains of D1 of PSII and PetB
485 of the Cytb₆f complex with CpSRP54 also exists (Nilsson *et al.*, 1999, Nilsson and van Wijk, 2002,
486 Piskozub *et al.*, 2015). A recent ribosome profiling study comparing thylakoid membrane association
487 of translating ribosomes between WT and a mutant lacking CpSRP54 further confirmed CpSRP54's
488 role in co-translational targeting of central photosynthetic proteins in plants (Hristou *et al.*, 2019).
489 Similar to the results described above, several chloroplast-encoded subunits of PSI, PSII, Cytb₆f and
490 ATP synthase were found at moderately lower levels in the *P. tricornutum cpsrp54* mutants. In *A.*
491 *thaliana*, the clearest effects of CpSRP54 depletion were seen on the level of PSI and PSII RC
492 proteins, whereas in *P. tricornutum* only the PSII RC protein D2 was significantly downregulated in
493 mutant lines. Despite some discrepancies in which subunits that were most severely affected by the
494 loss of CpSRP54, and that we have no evidence for direct interaction between CpSRP54 and
495 elongating thylakoid membrane proteins in *P. tricornutum*, the combined results from this study do
496 imply that CpSRP54 is involved, but not essential, in targeting of chloroplast-encoded proteins to
497 thylakoids in diatoms as well.

498

499 Effect of loss of CpSRP54 is alleviated by compensating mechanisms

500 The relatively mild phenotype of both the *A. thaliana* and *P. tricornutum cpsrp54* mutants might be
501 partially explained by execution of compensation mechanisms involving the upregulation of
502 chaperones that can alleviate the effects of loss of CpSRP54. Absence of CpSRP54 resulted in
503 upregulation of DnaK homologs cpHSP70-1/2, CPN60 proteins, co-chaperonin CPN21 and ClpC-1/2
504 in *A. thaliana* (Rutschow *et al.*, 2008) and elevated levels of DnaK, DnaJ and ClpB in *P. tricornutum*.
505 Upregulations of a range of cytoplasmic chaperons belonging mostly to the same families as the ones
506 found in the chloroplastic responses, have also been reported as a common response to the loss of

507 cytoplasmic SRP54 in yeast and bacteria (Arnold and Wittrup, 1994, Mutka and Walter, 2001,
508 Wickström *et al.*, 2011, Zhang *et al.*, 2012). Here, upregulation of the chaperone systems is believed
509 to prevent the accumulation of mis-localized and aggregated proteins and might provide alternative
510 pathways to target proteins to its target membranes (Arnold and Wittrup, 1994, Mutka and Walter,
511 2001, Wickström *et al.*, 2011, Zhang *et al.*, 2012). Although no functional data is available about
512 roles and interaction partners of the chloroplast-localized DnaK in diatoms, the ~3-fold upregulation
513 of the *P. tricornutum* DnaK in *cpsrp54* lines compared to WT suggests key roles for this
514 multifunctional chaperon in coping with the stress of lacking CpSRP54. The simultaneous
515 upregulation of DnaK, its putative cochaperone DnaJ and of one of their possible interaction partners,
516 the diatom VIPP1 homolog, as a response to the lack of CpSRP54 opens for speculations about an
517 indirect role of DnaK in insertion of thylakoid membrane proteins. As previously mentioned, the
518 exact function of VIPP1 beyond its importance in thylakoid membrane biogenesis/maintenance is
519 unclear, but one of its many suggested roles is connected to insertion of photosynthetic proteins
520 (Bryan *et al.*, 2014, Trösch *et al.*, 2015, Heidrich *et al.*, 2017, Gutu *et al.*, 2018). In plants, VIPP1 has
521 been detected as a component of D1 intermediates together with CpSRP54, CpFTSY, ALB3 and
522 CpSecY, and found to stimulate insertion of D1 (Walter *et al.*, 2015a). Depletion of the ALB3.2
523 insertase of the co-translational CpSRP pathway in *C. reinhardtii* resulted in upregulation of VIPP1,
524 the DnaK homolog HSP70B and its cochaperone (Göhre *et al.*, 2006). VIPP1 is also upregulated in
525 *C. reinhardtii* mutants lacking the ALB3.1 insertase mainly involved in the posttranslational
526 insertions of LHCPs, but absence of ALB3.1 also causes lower levels of D1 (Bellafiore *et al.*, 2002,
527 Theis *et al.*, 2020). In addition, both HSP70B and VIPP1 are high light inducible and indicated to be
528 involved in PSII repair in *C. reinhardtii* (Drzymalla *et al.*, 1996, Nordhues *et al.*, 2012, Trösch *et al.*,
529 2015). A possible connection between DnaK-type chaperones, VIPP1 and PS biogenesis has been
530 suggested where the chaperones influence the activity of VIPP1 by catalyzing the assembly and
531 disassembly of the VIPP1 oligomers, and where VIPP1 provides local areas where PS biogenesis can
532 take place (Liu *et al.*, 2007, Rütgers and Schroda, 2013, Bryan *et al.*, 2014, Trösch *et al.*, 2015, Gutu
533 *et al.*, 2018). A similar role in PS biogenesis for the DnaK-type chaperone system and VIPP1 in
534 diatoms is imaginable, but no functional data is currently available to support such speculations.

535

536

537 Conclusion

538 Previous studies of the effects of loss of CpSRP54 in model organisms representing land plants and
539 green microalgae and the current study of the effect of loss of CpSRP54 in the model diatom *P.*
540 *tricornutum* show that although there are some similarities (see overview in Table 3), the mechanisms
541 for targeting proteins to thylakoid membranes are too different for a direct transfer of knowledge from
542 one group of species to another. A schematic representation of the CpSRP pathway for integration of
543 thylakoid membrane proteins in *P. tricornutum* compared to plants (*A. thaliana*) and green algae (*C.*
544 *reinhardtii*) is given in Figure 7. Major differences exist for the role of CpSRP54 in the three model
545 systems. In *P. tricornutum* we suggest that CpSRP54, likely in interaction with the CpFTSY receptor,
546 guides translating ribosomes to the ALB3a insertase (and possibly the CpSecY translocase) for co-
547 translational insertion of chloroplast-encoded thylakoid membrane proteins (Figure 7A, right side) in
548 a similar manner as the CpSRP54 of *A. thaliana* (Figure 7B, right side) (Ziehe *et al.*, 2018). *A.*
549 *thaliana* CpSRP54 has a dual function and targets also LHCPs to thylakoid membranes (Figure 7B,
550 left side). The role(s) of CpSRP54 in *P. tricornutum* and *A. thaliana* contrasts with the role of
551 CpSRP54 in *C. reinhardtii*, which is reported to function exclusively in the post-translational
552 insertion of LHCPs (Figure 7C, left side) (Jeong *et al.*, 2017). CpSRP54 and other members of the
553 CpSRP pathway (CpFTSY and CpSRP43) have been suggested to be suitable universal targets for
554 gene editing with the purpose of minimizing the chlorophyll antenna size in microalgae because of
555 their role in the post-translational part of the CpSRP pathway in *C. reinhardtii* (Kirst and Melis, 2014,
556 Jeong *et al.*, 2017). Truncation of the light harvesting antenna in green microalgae causes improved
557 rates of growth and productivity under high-density and bright sunlight conditions, features that are
558 desired from a commercial point of view (Kirst and Melis, 2014, Jeong *et al.*, 2017). The data
559 presented above clearly show that such a phenotype is not achieved by disrupting the gene encoding
560 CpSRP54 in *P. tricornutum*, and our data is only in support of a role for the CpSRP54 in the co-
561 translational insertion of chloroplast-encoded proteins. Targeting of diatom FCP proteins to thylakoid
562 membranes seems to be independent of the CpSRP pathway (Figure 7A, left side), making it unlikely
563 that members of this pathway can be exploited in strain optimization for high density cultivation of
564 diatoms.

565 Experimental procedures

566 The axenic *P. tricornutum* Bohlin clone Pt1 8.6 (CCMP632) culture was obtained from the culture
567 collection of the Provasoli-Guillard National Center for Culture of Marine Phytoplankton, Bigelow
568 Laboratory for Ocean Sciences, USA.

569 *P. tricornutum cpsrp54* knock out mutants

570 The *cpsrp54-8*, *cpsrp54-11*, *cpsrp54-20* mutant lines used for this study were isolated from single
571 cells from the M2, M4 and M8 lines, respectively, previously published in Nymark et al. (Nymark et
572 al., 2016). The *cpsrp54* KO mutants had been created with the aid of the CRISPR/Cas9 technology
573 using a *P. tricornutum* culture derived from the sequenced clone Pt1 8.6 (Bowler et al., 2008) as a
574 starting point. Knock out mutations were confirmed in the three lines by TOPO cloning and
575 subsequent Sanger sequencing of PCR products spanning the region of the *CpSRP54* gene targeted
576 by the Cas9-gRNA complex as described previously (Nymark et al., 2016, Nymark et al., 2017)

578 Growth and experimental light conditions

579 *P. tricornutum* wild type (WT) cells and *cpsrp54* lines (*cpsrp54-8*, *cpsrp54-11*, *cpsrp54-20*) were
580 cultured as described previously (Nymark et al., 2009). Cell cultures were grown at 15°C under
581 continuous cool white fluorescent light at scalar irradiance (E_{PAR}) of $\sim 35 \mu\text{mol photons m}^{-2} \text{s}^{-1}$ (low
582 light (LL)) or $\sim 200 \mu\text{mol photons m}^{-2} \text{s}^{-1}$ (medium light (ML)), unless stated otherwise. High light
583 (HL; $\sim 1000 \mu\text{mol photons m}^{-2} \text{s}^{-1}$) was provided by a full spectrum LED lamp (5500 K). The
584 cultures were kept in the exponential growth phase for at least two weeks under LL, ML or HL
585 conditions before conducting experiments.

586 Growth rates

587 Growth rates were estimated in batch cultures of WT and *cpsrp54* KO lines (three biological
588 replicates) acclimated to LL, ML or HL. The starting concentrations used for determining the
589 growth rates were 200.000 cells/ml for LL-acclimated cells, 100.000 cells/ml for ML-acclimated
590 cells and 50.000 cells/ml for HL-acclimated cells. Cells were fixed in Lugol's solution and counted
591 by using a Bürker-Türk counting chamber or by flowcytometry as described previously (Nymark et
592 al., 2016). The average maximum growth rates (cell division/day) for WT and mutant lines were
593 calculated by using the mean of the growth rates from the three biological replicates during the
594 exponential phase.

595

596 *In vivo* fluorescence excitation

597 *In vivo* fluorescence excitation spectra were obtained from LL-acclimated WT and *cpsrp54* cultures
598 (three biological replicates) using a Hitachi F-3000 spectrofluorometer (Hitachi Corp.) as previously
599 described (Johnsen and Sakshaug, 2007, Nymark *et al.*, 2013). Excitation light was provided at 1 nm
600 spectral resolution (5 nm bandwidth) from 400 to 700 nm, registering Chl *a* fluorescence emission at
601 730 nm (5 nm band width) as a function of absorbed light at the different wavelengths. 3-(3,4-
602 dichlorophenyl)-1,1-dimethylurea (DCMU; 50 μ M final concentration) was added 1 minute prior to
603 each measurement to avoid variable fluorescence. All spectra were normalized to the red emission
604 maximum of Chl *a* of the WT cultures.

605

606 Absorbance spectra

607 Absorption spectra were measured with a Multiscan sky spectrophotometer (Thermo Fisher
608 Scientific, USA) with a resolution of 1 nanometer. Cells were loaded on a multiwell plate and spectra
609 were normalized on the blue absorption peak. Data are representative of 3 biological replicates (3
610 technical replicates per genotype per experiment).

611

612 LL to ML shift time-series experiments

613 LL acclimated (0 h) *cpsrp54* KO lines were exposed to ML for 0.5, 6, 24, 48 h and 168 h. Three
614 biological replicates were included for each line and time point. Cell concentrations were approx. 1
615 $\times 10^6$ cells/mL at the day of harvesting. Harvested material was used for monitoring of the
616 photophysiological state and pigment concentration per cell in LL and after the shift to ML. The time-
617 series experiment in the current study and in a previously published study characterizing the *P.*
618 *tricornutum alb3b* mutant (Nymark *et al.*, 2019) were performed in parallel and the responses of the
619 *cpsrp54* and *alb3b* mutants were therefore compared to the same WT dataset.

620

621 Pigment analysis

622 Pigment analysis were performed by HPLC according to Rodriguez *et al.* (Rodriguez *et al.*, 2006)
623 using a Hewlett-Packard HPLC 1100 Series system. Pigment values from the HPLC analysis were
624 calculated as femtomol (fmol) pigment per cell. Cell concentrations were determined using a BD
625 Accuri C6 Flow Cytometer as described previously (Nymark *et al.*, 2019).

626 Measurements of photosynthetic parameters

627 Variable *in vivo* Chl *a* fluorescence was measured as described in Nymark et al. (Nymark *et al.*, 2019)
628 using a PhytoPAM (System I, Walz, Germany) equipped with a photomultiplier detector (PM-101P,
629 Walz, Germany). The photosynthetic efficiency (F_v/F_m), the photosynthetic capacity (maximum
630 relative electron transport rate ($rETR_{max}$), the maximum light utilization coefficient (α), the light
631 saturation index ($E_k=rETR_{max}/\alpha$) and NPQ were calculated as described previously (Nymark *et al.*,
632 2009, Nymark *et al.*, 2019). NPQ data was derived from light response curves from LL-acclimated
633 cultures. All samples were incubated 3 min in darkness prior to performing measurements. A Peltier
634 cell (US-T/S, Walz) kept the temperature at 15°C ($\pm 0.2^\circ\text{C}$) during the measurements.

635 The ECS signal in LL and ML-acclimated cells was measured with a Joliot-type spectrophotometer
636 (JTS-10, Biologic) equipped with a laser or xenon lamp as excitation sources, white probing light and
637 interference filters (3-8 nm bandwidth) allowing measurements of the absorption difference signals
638 at selected wavelengths (Bailleul *et al.*, 2015). All cultures were upconcentrated to 20 million cells/ml
639 by centrifugation prior to performing the measurements. Measurements of PSII/PSI stoichiometries
640 were measured under single turnover flash regime. ECS kinetics were triggered by excitation with a
641 saturating light flash produced by a laser or xenon lamp causing a single charge separation in all
642 active PSs. Three different phases were observed: a fast rise of the signal corresponding to charge
643 separation in PSI and PSII (<100 μs after laser flash), a slower rise (ms time range) representing
644 electron flow through Cyt_{b6}f and a decay phase due to charge leakage through the membrane (Bailleul
645 *et al.*, 2010). The linear component of the ECS (ECS_{lin}) was used to estimate the PSII/PSI ratio. ECS_{lin}
646 was deconvoluted from superimposed signals by measuring at three different wavelengths (520, 554
647 and 563 nm) as described in Bailleul et al. (Bailleul *et al.*, 2015). Briefly, we first assessed the
648 contribution of c-type cytochromes in the measured signal as $\text{Cyt } c = [554] - 0.4 \times [520] - 0.4 \times [563]$,
649 where [554], [520] and [566] were the measured absorption difference signals at the three different
650 wavelengths. Secondly, we evaluated ECS_{lin} as $= [520] - 0.25 \times \text{Cyt } c$. PSII contribution was
651 evaluated from the amplitude of the fast ECS_{lin} phase as the decrease in the signal amplitude upon
652 poisoning samples with DCMU (20 μM) and hydroxylamine (HA; 1 mM) to irreversibly block PSII
653 charge separation. PSI was estimated as the fraction of the signal that was insensitive to these
654 inhibitors (Bailleul *et al.*, 2010).

655 The same approach was used to evaluate photosynthetic electron flow (electrons per second) in LL

656 and ML-acclimated WT and *cpsrp54* cells. Cells were illuminated with continuous red light (590
657 $\mu\text{mol photons m}^{-2} \text{ s}^{-1}$) until steady state photosynthesis was achieved. Then, light was switched off
658 and the rate of photosynthetic electron flow was measured as described in (Bailleul *et al.*, 2010).
659 Briefly, in steady state the ECS signal reflects membrane potential generation by the PSs and Cytb₆f
660 complex and membrane potential dissipation by the ATP synthase. When light is switched off, PSII
661 and PSI activity stops abruptly, while ATP synthase and the Cytb₆f complex activities remain
662 (transiently) unchanged. Therefore, the difference between the slopes of the ECS signal measured in
663 the light and after the light is switched off is proportional to the rate of PSI and PSII photochemistry
664 (i.e. to the rate of electron flow). This rate can be quantified by dividing the slope difference by the
665 amplitude of the fast ECS_{in} phase measured under single turnover flashes in the presence of DCMU
666 and HA. The latter reflects the ECS absorption changes induced by the transfer of a single charge
667 across the membrane (e.g. one electron per photosynthetic chain).

668 High light lincomycin experiment

669 Lincomycin (LINC; Sigma-Aldrich) blocks chloroplast protein synthesis (Ridley and Ridley, 1979)
670 and was added to LL-acclimated cultures (3 biological replicates) in the exponential phase at a final
671 concentration of 500 $\mu\text{g mL}^{-1}$. Cultures were incubated in darkness for 15 min before exposure to HL
672 (1000 $\mu\text{mol photons m}^{-2} \text{ s}^{-1}$) for 1 h. In parallel, cultures without LINC were exposed to the same
673 treatment. F_v/F_m was measured in LL and HL treated cultures using an AquaPen-C (Photon System
674 Instruments). LL acclimated cells were incubated in darkness for 3 min prior to measurements,
675 whereas HL-treated cells were measured after both a 3 min and 30 min very dim light period. The
676 additional measurement after 30 min was included to relax the rapidly reversible qE component of
677 NPQ so that only the photoinhibitory, slowly reversible quenching (qI), caused by damaged PSII
678 reaction centers, would influence the F_v/F_m value.

679

680 Proteomics

681 Proteomic analyses were performed of *cpsrp54-8*, *cpsrp54-11* and WT lines after 6 h exposure to
682 ML. Five biological replicates were included for each line, and cells were harvested by filtration as
683 described previously (Nymark *et al.*, 2019). To each sample, 100 μl of SDC buffer (1% SDC, 10 mM
684 TCEP, 40 mM 2-Chloroacetamide, Roche Protease Inhibitor cocktail, 100 mM Tris pH 8.5) was
685 added. After mixing by pipetting, contents were transferred to LoBind tubes (Eppendorf), the tubes
686 were kept at 95 °C for 5 minutes, before being sonicated at 4 °C in a Bioruptor Pico (Diagenode) for

687 10 cycles, each with 1 min sonication followed by 30 sec without sonication. Protein concentration
688 was measured in a Direct Detect (Millipore) and a volume containing 50 µg total protein was
689 separated for further sample preparation. The volume was adjusted to 50 µl by addition of water.
690 Next, a KingFisher Flex (Thermo Scientific) magnetic-bead handling robot performed clean-up of
691 the proteins using HILIC magnetic microparticles (ReSyn Bioscience) followed by tryptic digestion
692 into peptides. In more details, deep well plates were prepared and placed into the KingFisher as: 25
693 µl of HILIC microparticles (20 mg/ml) and 175 µl Equilibration buffer (15% Acetonitrile, 100 mM
694 Ammonium acetate pH 4.5) at position 1, 500 µl Equilibration buffer at position 2, 50 µl sample and
695 50 µl Bind buffer (0.5% SDS, 30% Acetonitrile, 200 mM Ammonium acetate pH 4.5) at position 3,
696 200 µl 95% Acetonitrile at positions 4 and 5, 50 µl Trypsin (0.1 µg/µl in 45 mM Acetic Acid) and
697 150 µl Digestion buffer (20 mM Ammonium formate pH 8.2) at position 6, comb Tip at position 7.
698 Then the robot executed the following protocol: picked up the comb tip, collected HILIC magnetic
699 particles, equilibrated HILIC magnetic particles in Equilibration buffer, bound protein to HILIC
700 magnetic particles, washed in high organic content twice, eluted from HILIC and digested protein
701 with Trypsin at 37° for 4 hours, removed HILIC magnetic particles. BindIt Software 3.3.1 (Thermo
702 Scientific) was used to prepare the robot protocol and to run it. Unless otherwise-stated, chemicals
703 were from Sigma.

704 Subsequently the digested peptides were transferred to new tubes, they were acidified by addition of
705 2 µl formic acid, then the tubes were spun-down (16,000g for 5 min) and 100 µl of supernatants were
706 transferred to LC-MS vials. Analysis was performed on an EASY-nLC 1200 UHPLC system (Thermo
707 Scientific) interfaced with an Q Exactive HF mass spectrometer (Thermo Scientific) via a Nanospray
708 Flex ion source (Thermo Scientific). Peptides were injected onto an Acclaim PepMap100 C18 trap
709 column (75 µm i.d., 2 cm long, 3 µm, 100 Å, Thermo Scientific) and further separated on an Acclaim
710 PepMap100 C18 analytical column (75 µm i.d., 50 cm long, 2 µm, 100 Å, Thermo Scientific) at 250
711 nl/min using a 180-minute gradient (145 min 5%-35% B, 15 min 35%-100% B, 20 min 100% B;
712 where A is 0.1 % formic acid and B is 0.1 % formic acid, 80% acetonitrile). Unless otherwise-stated,
713 chemicals were from Fisher Scientific.

714 Peptide ions were analysed in positive ion mode under data dependent acquisition using the following
715 parameters: Electrospray voltage 1.9 kV, HCD fragmentation with normalized collision energy 27.
716 Each MS scan (200 to 2000 m/z, 3e6 AGC target, profile) was acquired at a resolution of 60,000
717 FWHM, followed by 15,000 FWHM MS/MS scans (200 to 2000 m/z, 1.2 m/z isolation width, 1e5

718 AGC target, 48 ms maximum IT, centroid) triggered for the 15 most intense ions, with a 25 s dynamic
719 exclusion. Charge exclusion was set to unassigned, 1 and greater than 5.

720 Proteins were identified and quantified by processing the MS data using Thermo Scientific Proteome
721 Discoverer (Thermo Scientific) version 2.3/4. Preview version 2.3.5 from Protein Metrics
722 Incorporated (Kil *et al.*, 2011) was used to inspect the raw files to determine optimal search criteria.
723 Namely, following search parameters were used: enzyme specified as Trypsin with maximum two
724 missed cleavages allowed; Acetylation of Protein N-terminal with Met-loss (Bonissone *et al.*, 2013),
725 Oxidation of Methionine and Deamidation of Asparagine/Glutamine as dynamic post-translational
726 modification while Carbamidomethylation of Cysteine as static; Precursor mass-tolerance of 20 PPM
727 while Fragment mass-tolerance of 0.02 Dalton. Spectrum file RC, PD's node, was set up to query the
728 raw files against the *Phaeodactylum tricornutum* (strain CCAP 1055/1) downloaded from Uniprot
729 (<https://www.uniprot.org/proteomes/UP000000759>) in December 2018 and internal contaminants
730 database to recalibrate and detect features with the Minora node and Sequest (Eng *et al.*, 1994) search
731 engines available PD. For downstream analysis of these peptide-spectra-matches (PSM), both protein
732 and peptide identifications/PSM false-discovery-rate (FDR) was set to 1% as high and 5% as medium
733 confidence, thus only unique peptides with these confidences thresholds were used for final protein
734 group identification and label the level of confidence respectively. Each protein group abundance was
735 normalized by the total abundance of all identified peptides/PSM at the FDR mentioned earlier and
736 scaled on all average with Precursor Ion Quantifier node of PD.

737 Protein isolation, SDS-PAGE and Western blot analysis

738 Cell harvesting, total protein isolation, determination of protein concentration, SDS-PAGE and
739 Western blot analysis were performed as previously described (Nymark *et al.*, 2019) using material
740 from WT and *cpsrp54* cultures acclimated to either LL or ML. Proteins were detected with the
741 following antibodies: anti-D1 (AS05 084 Agrisera; 1:20000 dilution), anti-D2 (AS06 146 Agrisera;
742 1:5000), anti-AtpB (AS05 085, Agrisera; 1:4000) and anti-LHCF1-11 (1:1000) (kind gift from C.
743 Büchel, University of Frankfurt, Germany; (Juhas *et al.*, 2014). Primary antibody incubation was
744 performed overnight at 4°C for all antibodies. Secondary antibody incubation was performed for 2 h
745 at room temperature using Goat anti-Rabbit IgG (H+L) Secondary Antibody, HRP conjugate
746 (ThermoFisher, 1:10000). Proteins were detected with SuperSignal West Pico PLUS
747 Chemiluminescent Substrate (Thermo Scientific) and the blots were imaged using a G:BOX
748 ChemiXRQ gel doc system (Syngene).

749 [Statistical analysis](#)

750 The R package ROTS (reproducibility-optimized test statistic) was used for statistical analysis of the
751 proteomics data aiming to identify differentially expressed proteins in *cpsrp54-8* and *cpsrp54-11*
752 compared to WT after 6 h exposure to ML (Suomi *et al.*, 2017). ROTS employs a bootstrapping
753 method to identify the proper t-test statistics based on the data. Prior to the differential expression
754 analysis, the intensity counts were normalized across samples. Additionally, for the validity of the
755 results, the homogeneity in pair-wise and group-wise variances was tested using an F-test and a p-
756 value of 0.05 as a significance threshold. Once normality and homogeneity in variance were ensured,
757 two independent tests were performed; one for WT against *cpsrp54-8* and one for WT against
758 *cpsrp54-11*. The differential expression analysis was performed using log₂ transformed values, while
759 proteins with only one abundance value across the samples were omitted. For both tests, the number
760 of bootstrapping and the number of top-ranked features for reproducibility optimization were set to
761 1000.

762 Two-way ANOVA with Dunnet's multiple comparison tests were carried out using GraphPad Prism
763 Software (version 8.4.3) to determine if there were significant differences (p<0.05) between the
764 pigment levels and photosynthetic parameters in *cpsrp54* mutants compared to WT.

765 [Accession numbers](#)

766 The CpSRP54 gene has Draft ID Phatr2_35185 and NCBI accession number XM_002179577.
767 UniProt accession numbers for differentially expressed proteins discussed in the text are included in
768 Table 2. UniProt accession numbers are provided for all proteins detected by the proteomics analyses
769 and the data are deposited to the ProteomeXchange Consortium as described below in the Data
770 availability statement.

771 [Data availability statement](#)

772 A complete submission of proteomics data including raw data (raw), peak-list (mzML),
773 identifications (mzID), workflow (pdAnalysis) and annotated results (xlsx) has been deposited to the
774 ProteomeXchange Consortium via the PRIDE (Perez-Riverol *et al.*, 2019) partner repository with the
775 dataset identifier PXD020167 and 10.6019/PXD020167. All other relevant information can be found
776 within the manuscript and its supporting information.

777 [Acknowledgements](#)

778 We wish to thank Kjersti Andresen for assistance with the HPLC analyses and Professor Claudia

779 Büchel for kindly providing LHCF antibodies. The authors would also like to thank Stoyan Stoychev
780 at ReSyn Bioscience for helpful discussions on the HILIC sample preparation protocol, and Felicity
781 Ashcroft for help with statistical analyses.

782 [Author contributions](#)

783 M.N., P.W. and A.M.B. conceived the research plans. M.N., P.W. and G.F. supervised and designed
784 the experiments. M.N., M.C.G.H., C.V., D.M.F., M.S. and G.F. performed the experiments. M.N.,
785 M.C.G.H., C.V., D.M.F., A.S., E.T., P.W. and G.F. analyzed the data. M.N. wrote the article with
786 contributions from co-authors. M.N. agrees to serve as the author responsible for contact and ensures
787 communication.

788

789 [Funding](#)

790 This work was supported by a grant from the Research Council of Norway to A.M.B through funding
791 of the project “Downsizing light harvesting antennae to scale up production potential and valorization
792 from cultivation of marine microalgae” (project no. 267474), to Olav Vadstein through funding of
793 the project Microbially Produced Raw Materials for Aquafeed (project no. 239001) and the NTNU
794 enabling technologies program to P.W.

795 [Conflict of interest](#)

796 The authors declare that they have no competing interests.

797

798 [Supporting information](#)

799 **Figure S1.** DNA sequence alignments of the *cpsrp54* mutant lines.

800 **Figure S2.** Overview of blots used for calculations of LHCF1-11 protein expression levels in WT
801 and *cpsrp54* lines acclimated to LL and ML.

802 **Figure S3.** Overview of blots used for calculations of D1 protein expression levels in WT and
803 *cpsrp54* lines grown in LL or ML.

804 **Figure S4.** Overview of blots used for calculations of D2 protein expression levels in WT and
805 *cpsrp54* lines grown in LL or ML.

806 **Supplementary Dataset 1.** Significantly regulated proteins comprising the photosynthetic
807 apparatus.

808 References

- 809 Amin, P., Sy, D.A., Pilgrim, M.L., Parry, D.H., Nussaume, L. and Hoffman, N.E. (1999)
810 Arabidopsis mutants lacking the 43- and 54-kilodalton subunits of the chloroplast signal
811 recognition particle have distinct phenotypes. *Plant Physiol*, **121**, 61-70.
812 <https://doi.org/10.1104/pp.121.1.61>
- 813 Armbrust, E.V. (2009) The life of diatoms in the world's oceans. *Nature*, **459**, 185-192.
814 <https://doi.org/10.1038/nature08057>
- 815 Arnold, C.E. and Wittrup, K.D. (1994) The stress response to loss of signal recognition particle
816 function in *Saccharomyces cerevisiae*. *J Biol Chem*, **269**, 30412-30418
- 817 Aro, E.M., Suorsa, M., Rokka, A., Allahverdiyeva, Y., Paakkarinen, V., Saleem, A.,
818 Battchikova, N. and Rintamaki, E. (2005) Dynamics of photosystem II: a proteomic
819 approach to thylakoid protein complexes. *J Exp Bot*, **56**, 347-356.
820 <https://doi.org/10.1093/jxb/eri041>
- 821 Aro, E.M., Virgin, I. and Andersson, B. (1993) Photoinhibition of Photosystem II. Inactivation,
822 protein damage and turnover. *Biochim Biophys Acta*, **1143**, 113-134.
823 [https://doi.org/10.1016/0005-2728\(93\)90134-2](https://doi.org/10.1016/0005-2728(93)90134-2)
- 824 Bachmann, K.M., Ebbert, V., Adams, W.W., Verhoeven, A.S., Logan, B.A. and Demmig-
825 Adams, B. (2004) Effects of lincomycin on PSII efficiency, non-photochemical quenching,
826 D1 protein and xanthophyll cycle during photoinhibition and recovery. *Funct Plant Biol*, **31**,
827 803-813. <https://doi.org/10.1071/Fp04022>
- 828 Bailleul, B., Berne, N., Murik, O., Petroustos, D., Prihoda, J., Tanaka, A., Villanova, V., Bligny,
829 R., Flori, S., Falconet, D., Krieger-Liszak, A., Santabarbara, S., Rappaport, F., Joliot,
830 P., Tirichine, L., Falkowski, P.G., Cardol, P., Bowler, C. and Finazzi, G. (2015) Energetic
831 coupling between plastids and mitochondria drives CO₂ assimilation in diatoms. *Nature*, **524**,
832 366-369. <https://doi.org/10.1038/nature14599>
- 833 Bailleul, B., Cardol, P., Breyton, C. and Finazzi, G. (2010) Electrochromism: a useful probe to
834 study algal photosynthesis. *Photosynth Res*, **106**, 179-189. <https://doi.org/10.1007/s11120-010-9579-z>
- 835
- 836 Bellafiore, S., Ferris, P., Naver, H., Gohre, V. and Rochaix, J.D. (2002) Loss of Albino3 leads to
837 the specific depletion of the light-harvesting system. *Plant Cell*, **14**, 2303-2314
- 838 Bethmann, S., Melzer, M., Schwarz, N. and Jahns, P. (2019) The zeaxanthin epoxidase is degraded
839 along with the D1 protein during photoinhibition of photosystem II. *Plant Direct*, **3**.
840 <https://doi.org/10.1002/pld3.185>
- 841 Bonissone, S., Gupta, N., Romine, M., Bradshaw, R.A. and Pevzner, P.A. (2013) N-terminal
842 protein processing: a comparative proteogenomic analysis. *Mol Cell Proteomics*, **12**, 14-28.
843 <https://doi.org/10.1074/mcp.M112.019075>
- 844 Bowler, C., Allen, A.E., Badger, J.H., Grimwood, J., Jabbari, K., Kuo, A., Maheswari, U.,
845 Martens, C., Maumus, F., Otiillar, R.P., Rayko, E., Salamov, A., Vandepoele, K.,
846 Beszteri, B., Gruber, A., Heijde, M., Katinka, M., Mock, T., Valentin, K., Verret, F.,
847 Berges, J.A., Brownlee, C., Cadoret, J.P., Chiovitti, A., Choi, C.J., Coesel, S., De
848 Martino, A., Detter, J.C., Durkin, C., Falciatore, A., Fournet, J., Haruta, M., Huysman,
849 M.J., Jenkins, B.D., Jiroutova, K., Jorgensen, R.E., Joubert, Y., Kaplan, A., Kroger, N.,
850 Kroth, P.G., La Roche, J., Lindquist, E., Lommer, M., Martin-Jezequel, V., Lopez, P.J.,
851 Lucas, S., Mangogna, M., McGinnis, K., Medlin, L.K., Montsant, A., Oudot-Le Secq,
852 M.P., Napoli, C., Obornik, M., Parker, M.S., Petit, J.L., Porcel, B.M., Poulsen, N.,
853 Robison, M., Rychlewski, L., Rynearson, T.A., Schmutz, J., Shapiro, H., Siat, M.,

- 854 Stanley, M., Sussman, M.R., Taylor, A.R., Vardi, A., von Dassow, P., Vyverman, W.,
855 Willis, A., Wyrwicz, L.S., Rokhsar, D.S., Weissenbach, J., Armbrust, E.V., Green, B.R.,
856 Van de Peer, Y. and Grigoriev, I.V. (2008) The *Phaeodactylum* genome reveals the
857 evolutionary history of diatom genomes. *Nature*, **456**, 239-244.
858 <https://doi.org/10.1038/nature07410>
- 859 Bozarth, A., Maier, U.G. and Zauner, S. (2009) Diatoms in biotechnology: modern tools and
860 applications. *Appl Microbiol Biotechnol*, **82**, 195-201. [https://doi.org/10.1007/s00253-008-](https://doi.org/10.1007/s00253-008-1804-8)
861 [1804-8](https://doi.org/10.1007/s00253-008-1804-8)
- 862 Brembu, T., Winge, P., Tooming-Klunderud, A., Nederbragt, A.J., Jakobsen, K.S. and Bones,
863 A.M. (2014) The chloroplast genome of the diatom *Seminavis robusta*: new features
864 introduced through multiple mechanisms of horizontal gene transfer. *Mar Genomics*, **16**, 17-
865 27. <https://doi.org/10.1016/j.margen.2013.12.002>
- 866 Bryan, S.J., Burroughs, N.J., Shevela, D., Yu, J., Rupprecht, E., Liu, L.N., Mastroianni, G.,
867 Xue, Q., Llorente-Garcia, I., Leake, M.C., Eichacker, L.A., Schneider, D., Nixon, P.J.
868 and Mullineaux, C.W. (2014) Localisation and interactions of the Vipp1 protein in
869 cyanobacteria. *Mol Microbiol*. <https://doi.org/10.1111/mmi.12826>
- 870 Butler, T., Kapoore, R.V. and Vaidyanathan, S. (2020) *Phaeodactylum tricorutum*: A diatom cell
871 factory. *Trends Biotechnol*, **38**, 606-622. <https://doi.org/10.1016/j.tibtech.2019.12.023>
- 872 Chandrasekar, S. and Shan, S.O. (2017) Anionic phospholipids and the Albino3 translocase
873 activate signal recognition particle-receptor interaction during light-harvesting chlorophyll
874 *a/b*-binding protein targeting. *J Biol Chem*, **292**, 397-406.
875 <https://doi.org/10.1074/jbc.M116.752956>
- 876 Dall'Osto, L., Caffarri, S. and Bassi, R. (2005) A mechanism of nonphotochemical energy
877 dissipation, independent from PsbS, revealed by a conformational change in the antenna
878 protein CP26. *Plant Cell*, **17**, 1217-1232. <https://doi.org/10.1105/tpc.104.030601>
- 879 Dittami, S.M., Michel, G., Collen, J., Boyen, C. and Tonon, T. (2010) Chlorophyll-binding
880 proteins revisited—a multigenic family of light-harvesting and stress proteins from a brown
881 algal perspective. *BMC Evol Biol*, **10**, 365. <https://doi.org/10.1186/1471-2148-10-365>
- 882 Doyle, S.M., Shastry, S., Kravats, A.N., Shih, Y.H., Miot, M., Hoskins, J.R., Stan, G. and
883 Wickner, S. (2015) Interplay between *E. coli* DnaK, ClpB and GrpE during protein
884 disaggregation. *J Mol Biol*, **427**, 312-327. <https://doi.org/10.1016/j.jmb.2014.10.013>
- 885 Drzymalla, C., Schroda, M. and Beck, C.F. (1996) Light-inducible gene HSP70B encodes a
886 chloroplast-localized heat shock protein in *Chlamydomonas reinhardtii*. *Plant Mol Biol*, **31**,
887 1185-1194. <https://doi.org/10.1007/BF00040835>
- 888 Dünschede, B., Träger, C., Schröder, C.V., Ziehe, D., Walter, B., Funke, S., Hofmann, E. and
889 Schünemann, D. (2015) Chloroplast SRP54 was recruited for posttranslational protein
890 transport via complex formation with chloroplast SRP43 during land plant evolution. *J Biol*
891 *Chem*, **290**, 13104-13114. <https://doi.org/10.1074/jbc.M114.597922>
- 892 Eng, J.K., McCormack, A.L. and Yates, J.R. (1994) An approach to correlate tandem mass spectral
893 data of peptides with amino acid sequences in a protein database. *J Am Soc Mass Spectrom*,
894 **5**, 976-989. [https://doi.org/10.1016/1044-0305\(94\)80016-2](https://doi.org/10.1016/1044-0305(94)80016-2)
- 895 Falk, S., Ravaud, S., Koch, J. and Sinning, I. (2010) The C terminus of the Alb3 membrane
896 insertase recruits cpSRP43 to the thylakoid membrane. *J Biol Chem*, **285**, 5954-5962.
897 <https://doi.org/10.1074/jbc.M109.084996>
- 898 Flori, S., Jouneau, P.H., Finazzi, G., Marechal, E. and Falconet, D. (2016) Ultrastructure of the
899 periplastidial compartment of the diatom *Phaeodactylum tricorutum*. *Protist*, **167**, 254-267.
900 <https://doi.org/10.1016/j.protis.2016.04.001>

- 901 **Fu, A., He, Z.Y., Cho, H.S., Lima, A., Buchanan, B.B. and Luan, S.** (2007) A chloroplast
902 cyclophilin and maintenance of functions in the assembly photosystem II in *Arabidopsis*
903 *thaliana*. *P Natl Acad Sci USA*, **104**, 15947-15952. <https://doi.org/10.1073/pnas.0707851104>
904 **Funke, S., Knechten, T., Ollesch, J. and Schünemann, D.** (2005) A unique sequence motif in the
905 54-kDa subunit of the chloroplast signal recognition particle mediates binding to the 43-kDa
906 subunit. *J Biol Chem*, **280**, 8912-8917. <https://doi.org/10.1074/jbc.M409992200>
907 **Gao, F., Wang, W.Y., Zhang, W.J. and Liu, C.M.** (2015) α -helical domains affecting the
908 oligomerization of Vipp1 and its interaction with Hsp70/DnaK in *Chlamydomonas*.
909 *Biochemistry*, **54**, 4877-4889. <https://doi.org/10.1021/acs.biochem.5b00050>
910 **Gibbs, S.P.** (1970) Comparative ultrastructure of algal chloroplast. *Ann Ny Acad Sci*, **175**, 454-+.
911 <https://doi.org/10.1111/j.1749-6632.1970.tb45167.x>
912 **Gibbs, S.P.** (1981) The chloroplasts of some algal groups may have evolved from endosymbiotic
913 eukaryotic algae. *Ann Ny Acad Sci*, **361**, 193-208. [https://doi.org/10.1111/j.1749-](https://doi.org/10.1111/j.1749-6632.1981.tb46519.x)
914 [6632.1981.tb46519.x](https://doi.org/10.1111/j.1749-6632.1981.tb46519.x)
915 **Gilbert, J.A., Field, D., Swift, P., Newbold, L., Oliver, A., Smyth, T., Somerfield, P.J., Huse, S.**
916 **and Joint, I.** (2009) The seasonal structure of microbial communities in the Western English
917 Channel. *Environ Microbiol*, **11**, 3132-3139. [https://doi.org/10.1111/j.1462-](https://doi.org/10.1111/j.1462-2920.2009.02017.x)
918 [2920.2009.02017.x](https://doi.org/10.1111/j.1462-2920.2009.02017.x)
919 **Goss, T. and Hanke, G.** (2014) The end of the line: Can ferredoxin and ferredoxin NADP(H)
920 oxidoreductase determine the fate of photosynthetic electrons? *Curr Protein Pept Sc*, **15**, 385-
921 393. <https://doi.org/10.2174/1389203715666140327113733>
922 **Grossman, A.R., Bhaya, D., Apt, K.E. and Kehoe, D.M.** (1995) Light-harvesting complexes in
923 oxygenic photosynthesis: diversity, control, and evolution. *Annu Rev Genet*, **29**, 231-288.
924 <https://doi.org/10.1146/annurev.ge.29.120195.001311>
925 **Grouneva, I., Gollan, P.J., Kangasjarvi, S., Suorsa, M., Tikkanen, M. and Aro, E.M.** (2013)
926 Phylogenetic viewpoints on regulation of light harvesting and electron transport in eukaryotic
927 photosynthetic organisms. *Planta*, **237**, 399-412. <https://doi.org/10.1007/s00425-012-1744-5>
928 **Gutu, A., Chang, F. and O'Shea, E.K.** (2018) Dynamical localization of a thylakoid membrane
929 binding protein is required for acquisition of photosynthetic competency. *Mol Microbiol*, **108**,
930 16-31. <https://doi.org/10.1111/mmi.13912>
931 **Göhre, V., Ossenbuhl, F., Crevecoeur, M., Eichacker, L.A. and Rochaix, J.D.** (2006) One of two
932 Alb3 proteins is essential for the assembly of the photosystems and for cell survival in
933 *Chlamydomonas*. *Plant Cell*, **18**, 1454-1466. <https://doi.org/10.1105/tpc.105.038695>
934 **Heidrich, J., Thurotte, A. and Schneider, D.** (2017) Specific interaction of IM30/Vipp1 with
935 cyanobacterial and chloroplast membranes results in membrane remodeling and eventually in
936 membrane fusion. *Bba-Biomembranes*, **1859**, 537-549.
937 <https://doi.org/10.1016/j.bbamem.2016.09.025>
938 **Hohmann-Marriott, M.F. and Blankenship, R.E.** (2011) Evolution of photosynthesis. *Annu Rev*
939 *Plant Biol*, **62**, 515-548. <https://doi.org/10.1146/annurev-arplant-042110-103811>
940 **Horn, A., Hennig, J., Ahmed, Y.L., Stier, G., Wild, K., Sattler, M. and Sinning, I.** (2015)
941 Structural basis for cpSRP43 chromodomain selectivity and dynamics in Alb3 insertase
942 interaction. *Nat Commun*, **6**, 8875. <https://doi.org/10.1038/ncomms9875>
943 **Hristou, A., Gerlach, I., Stolle, D.S., Neumann, J., Bischoff, A., Dunschede, B., Nowaczyk,**
944 **M.M., Zoschke, R. and Schunemann, D.** (2019) Ribosome-associated chloroplast SRP54
945 enables efficient cotranslational membrane insertion of key photosynthetic proteins. *Plant*
946 *Cell*, **31**, 2734-2750. <https://doi.org/10.1105/tpc.19.00169>
947 **Hutin, C., Havaux, M., Carde, J.P., Kloppstech, K., Meierhoff, K., Hoffman, N. and**

- 948 Nussaume, L. (2002) Double mutation cpSRP43/cpSRP54 is necessary to abolish the cpSRP
949 pathway required for thylakoid targeting of the light-harvesting chlorophyll proteins. *Plant J*,
950 **29**, 531-543. <https://doi.org/10.1046/j.0960-7412.2001.01211.x>
- 951 Jansen, M.A.K., Greenberg, B.M., Edelman, M., Mattoo, A.K. and Gaba, V. (1996) Accelerated
952 degradation of the D2 protein of photosystem II under ultraviolet radiation. *Photochem*
953 *Photobiol*, **63**, 814-817. <https://doi.org/10.1111/j.1751-1097.1996.tb09636.x>
- 954 Jeong, J., Baek, K., Kirst, H., Melis, A. and Jin, E. (2017) Loss of CpSRP54 function leads to a
955 truncated light-harvesting antenna size in *Chlamydomonas reinhardtii*. *Biochim Biophys Acta*
956 *Bioenerg*, **1858**, 45-55. <https://doi.org/10.1016/j.bbabi.2016.10.007>
- 957 Jeong, J., Baek, K., Yu, J., Kirst, H., Betterle, N., Shin, W., Bae, S., Melis, A. and Jin, E. (2018)
958 Deletion of the chloroplast LTD protein impedes LHCI import and PSI-LHCI assembly in
959 *Chlamydomonas reinhardtii*. *J Exp Bot*, **69**, 1147-1158. <https://doi.org/10.1093/jxb/erx457>
- 960 Johnsen, G. and Sakshaug, E. (2007) Biooptical characteristics of PSII and PSI in 33 species (13
961 pigment groups) of marine phytoplankton, and the relevance for pulse-amplitude-modulated
962 and fast-repetition-rate fluorometry. *J Phycol*, **43**, 1236-1251. <https://doi.org/10.1111/j.1529-8817.2007.00422.x>
- 963
- 964 Juhas, M., von Zadow, A., Spexard, M., Schmidt, M., Kottke, T. and Buchel, C. (2014) A novel
965 cryptochrome in the diatom *Phaeodactylum tricorutum* influences the regulation of light-
966 harvesting protein levels. *Febs J*, **281**, 2299-2311. <https://doi.org/10.1111/Febs.12782>
- 967 Junglas, B. and Schneider, D. (2018) What is Vipp1 good for? *Mol Microbiol*, **108**, 1-5.
968 <https://doi.org/10.1111/mmi.13924>
- 969 Järvi, S., Suorsa, M. and Aro, E.M. (2015) Photosystem II repair in plant chloroplasts - Regulation,
970 assisting proteins and shared components with photosystem II biogenesis. *Bba-Bioenergetics*,
971 **1847**, 900-909. <https://doi.org/10.1016/j.bbabi.2015.01.006>
- 972 Kil, Y.J., Becker, C., Sandoval, W., Goldberg, D. and Bern, M. (2011) Preview: a program for
973 surveying shotgun proteomics tandem mass spectrometry data. *Anal Chem*, **83**, 5259-5267.
974 <https://doi.org/10.1021/ac200609a>
- 975 Kirst, H., Formighieri, C. and Melis, A. (2014) Maximizing photosynthetic efficiency and culture
976 productivity in cyanobacteria upon minimizing the phycobilisome light-harvesting antenna
977 size. *Bba-Bioenergetics*, **1837**, 1653-1664. <https://doi.org/10.1016/j.bbabi.2014.07.009>
- 978 Kirst, H., Garcia-Cerdan, J.G., Zurbriggen, A. and Melis, A. (2012a) Assembly of the light-
979 harvesting chlorophyll antenna in the green alga *Chlamydomonas reinhardtii* requires
980 expression of the TLA2-CpFTSY gene. *Plant Physiol*, **158**, 930-945.
981 <https://doi.org/10.1104/pp.111.189910>
- 982 Kirst, H., Garcia-Cerdan, J.G., Zurbriggen, A., Ruehle, T. and Melis, A. (2012b) Truncated
983 photosystem chlorophyll antenna size in the green microalga *Chlamydomonas reinhardtii*
984 upon deletion of the TLA3-CpSRP43 gene. *Plant Physiol*, **160**, 2251-2260.
985 <https://doi.org/10.1104/pp.112.206672>
- 986 Kirst, H. and Melis, A. (2014) The chloroplast signal recognition particle (CpSRP) pathway as a
987 tool to minimize chlorophyll antenna size and maximize photosynthetic productivity.
988 *Biotechnol Adv*, **32**, 66-72. <https://doi.org/10.1016/j.biotechadv.2013.08.018>
- 989 Lang, M. and Kroth, P.G. (2001) Diatom fucoxanthin chlorophyll a/c-binding protein (FCP) and
990 land plant light-harvesting proteins use a similar pathway for thylakoid membrane Insertion.
991 *J Biol Chem*, **276**, 7985-7991. <https://doi.org/10.1074/jbc.M006417200>
- 992 Lavaud, J. and Goss, R. (2014) The peculiar features of non-photochemical fluorescence quenching
993 in diatoms and brown algae. In *Non-photochemical quenching and energy dissipation in*
994 *plants, algae and cyanobacteria. Advances in photosynthesis and respiration (Including*

995 *bioenergy and related processes*) (Demmig-Adams, B., Garab, G., Adams, I.W. and
996 Govindjee eds). Dordrecht: Springer, pp. 421-443.

997 **Levitan, O., Chen, M., Kuang, X., Cheong, K.Y., Jiang, J., Banal, M., Nambiar, N., Gorbunov,**
998 **M.Y., Ludtke, S.J., Falkowski, P.G. and Dai, W.** (2019) Structural and functional analyses
999 of photosystem II in the marine diatom *Phaeodactylum tricornutum*. *Proc Natl Acad Sci U S*
1000 *A*, **116**, 17316-17322. <https://doi.org/10.1073/pnas.1906726116>

1001 **Liu, C.M., Willmund, F., Golecki, J.R., Cacace, S., Hess, B., Markert, C. and Schroda, M.** (2007)
1002 The chloroplast HSP70B-CDJ2-CGE1 chaperones catalyse assembly and disassembly of
1003 VIPP1 oligomers in *Chlamydomonas*. *Plant J*, **50**, 265-277. [https://doi.org/10.1111/j.1365-](https://doi.org/10.1111/j.1365-313X.2007.03047.x)
1004 [313X.2007.03047.x](https://doi.org/10.1111/j.1365-313X.2007.03047.x)

1005 **Mishra, M., Arukha, A.P., Bashir, T., Yadav, D. and Prasad, G.B.K.S.** (2017) All new faces of
1006 diatoms: Potential source of nanomaterials and beyond. *Front Microbiol*, **8**.
1007 <https://doi.org/10.3389/fmicb.2017.01239>

1008 **Mishra, R.C. and Grover, A.** (2016) ClpB/Hsp100 proteins and heat stress tolerance in plants. *Crit*
1009 *Rev Biotechnol*, **36**, 862-874. <https://doi.org/10.3109/07388551.2015.1051942>

1010 **Mogk, A., Kummer, E. and Bukau, B.** (2015) Cooperation of Hsp70 and Hsp100 chaperone
1011 machines in protein disaggregation. *Front Mol Biosci*, **2**, 22.
1012 <https://doi.org/10.3389/fmolb.2015.00022>

1013 **Mutka, S.C. and Walter, P.** (2001) Multifaceted physiological response allows yeast to adapt to the
1014 loss of the signal recognition particle-dependent protein-targeting pathway. *Mol Biol Cell*, **12**,
1015 577-588. <https://doi.org/10.1091/mbc.12.3.577>

1016 **Nelson, D.M., Treguer, P., Brzezinski, M.A., Leynaert, A. and Queguiner, B.** (1995) Production
1017 and dissolution of biogenic silica in the ocean - Revised global estimates, comparison with
1018 regional data and relationship to biogenic sedimentation. *Global Biogeochem Cy*, **9**, 359-372.
1019 <https://doi.org/10.1029/95gb01070>

1020 **Nelson, N. and Ben-Shem, A.** (2004) The complex architecture of oxygenic photosynthesis. *Nat Rev*
1021 *Mol Cell Biol*, **5**, 971-982. <https://doi.org/10.1038/nrm1525>

1022 **Nilsson, R., Brunner, J., Hoffman, N.E. and van Wijk, K.J.** (1999) Interactions of ribosome
1023 nascent chain complexes of the chloroplast-encoded D1 thylakoid membrane protein with
1024 cpSRP54. *Embo J*, **18**, 733-742. <https://doi.org/10.1093/emboj/18.3.733>

1025 **Nilsson, R. and van Wijk, K.J.** (2002) Transient interaction of cpSRP54 with elongating nascent
1026 chains of the chloroplast-encoded D1 protein; 'cpSRP54 caught in the act'. *FEBS Lett*, **524**,
1027 127-133. [https://doi.org/10.1016/s0014-5793\(02\)03016-8](https://doi.org/10.1016/s0014-5793(02)03016-8)

1028 **Nordhues, A., Schottler, M.A., Unger, A.K., Geimer, S., Schonfelder, S., Schmollinger, S.,**
1029 **Rutgers, M., Finazzi, G., Soppa, B., Sommer, F., Muhlhaus, T., Roach, T., Krieger-**
1030 **Liszskay, A., Lokstein, H., Crespo, J.L. and Schroda, M.** (2012) Evidence for a role of
1031 VIPP1 in the structural organization of the photosynthetic apparatus in *Chlamydomonas*.
1032 *Plant Cell*, **24**, 637-659. <https://doi.org/10.1105/tpc.111.092692>

1033 **Nymark, M., Sharma, A.K., Hafskjold, M.C., Sparstad, T., Bones, A.M. and Winge, P.** (2017)
1034 CRISPR/Cas9 Gene editing in the marine diatom *Phaeodactylum tricornutum*. *Bio-protocol*
1035 **7**, e2442. <https://doi.org/10.21769/BioProtoc.2442>

1036 **Nymark, M., Sharma, A.K., Sparstad, T., Bones, A.M. and Winge, P.** (2016) A CRISPR/Cas9
1037 system adapted for gene editing in marine algae. *Sci Rep-Uk*, **6**.
1038 <https://doi.org/10.1038/srep24951>

1039 **Nymark, M., Valle, K.C., Brembu, T., Hancke, K., Winge, P., Andresen, K., Johnsen, G. and**
1040 **Bones, A.M.** (2009) An integrated analysis of molecular acclimation to high light in the
1041 marine diatom *Phaeodactylum tricornutum*. *PLoS ONE*, **4**, e7743.

- 1042 <https://doi.org/10.1371/journal.pone.0007743>
- 1043 **Nymark, M., Valle, K.C., Hancke, K., Winge, P., Andresen, K., Johnsen, G., Bones, A.M. and**
- 1044 **Brembu, T.** (2013) Molecular and photosynthetic responses to prolonged darkness and
- 1045 subsequent acclimation to re-illumination in the diatom *Phaeodactylum tricornutum*. *PLoS*
- 1046 *ONE*, **8**, e58722. <https://doi.org/10.1371/journal.pone.0058722>
- 1047 **Nymark, M., Volpe, C., Hafskjold, M.C.G., Kirst, H., Serif, M., Vadstein, O., Bones, A.M.,**
- 1048 **Melis, A. and Winge, P.** (2019) Loss of ALBINO3b insertase results in truncated light-
- 1049 harvesting antenna in diatoms. *Plant Physiol*, **181**, 1257-1276.
- 1050 <https://doi.org/10.1104/pp.19.00868>
- 1051 **Ouyang, M., Li, X., Ma, J., Chi, W., Xiao, J., Zou, M., Chen, F., Lu, C. and Zhang, L.** (2011)
- 1052 LTD is a protein required for sorting light-harvesting chlorophyll-binding proteins to the
- 1053 chloroplast SRP pathway. *Nat Commun*, **2**, 277. <https://doi.org/10.1038/ncomms1278>
- 1054 **Perez-Riverol, Y., Csordas, A., Bai, J.W., Bernal-Llinares, M., Hewapathirana, S., Kundu, D.J.,**
- 1055 **Inuganti, A., Griss, J., Mayer, G., Eisenacher, M., Perez, E., Uszkoreit, J., Pfeuffer, J.,**
- 1056 **Sachsenberg, T., Yilmaz, S., Tiwary, S., Cox, J., Audain, E., Walzer, M., Jarnuczak,**
- 1057 **A.F., Ternent, T., Brazma, A. and Vizcaino, J.A.** (2019) The PRIDE database and related
- 1058 tools and resources in 2019: improving support for quantification data. *Nucleic Acids Res*, **47**,
- 1059 D442-D450. <https://doi.org/10.1093/nar/gky1106>
- 1060 **Pilgrim, M.L., van Wijk, K.J., Parry, D.H., Sy, D.A. and Hoffman, N.E.** (1998) Expression of a
- 1061 dominant negative form of cpSRP54 inhibits chloroplast biogenesis in *Arabidopsis*. *Plant J*,
- 1062 **13**, 177-186. <https://doi.org/10.1046/j.1365-313x.1998.00021.x>
- 1063 **Piskozub, M., Kroliczewska, B. and Kroliczewski, J.** (2015) Ribosome nascent chain complexes
- 1064 of the chloroplast-encoded cytochrome b6 thylakoid membrane protein interact with cpSRP54
- 1065 but not with cpSecY. *J Bioenerg Biomembr*, **47**, 265-278. [https://doi.org/10.1007/s10863-](https://doi.org/10.1007/s10863-014-9598-0)
- 1066 [014-9598-0](https://doi.org/10.1007/s10863-014-9598-0)
- 1067 **Pool, M.R.** (2005) Signal recognition particles in chloroplasts, bacteria, yeast and mammals (review).
- 1068 *Mol Membr Biol*, **22**, 3-15. <https://doi.org/10.1080/09687860400026348>
- 1069 **Ridley, S.M. and Ridley, J.** (1979) Interaction of chloroplasts with inhibitors: Location of carotenoid
- 1070 synthesis and inhibition during chloroplast development. *Plant Physiol*, **63**, 392-398.
- 1071 <https://doi.org/10.1104/pp.63.2.392>
- 1072 **Ries, F., Herkt, C. and Willmund, F.** (2020) Co-translational protein folding and sorting in
- 1073 chloroplasts. *Plants-Basel*, **9**. <https://doi.org/10.3390/plants9020214>
- 1074 **Rodriguez, F., Chauton, M., Johnsen, G., Andresen, K., Olsen, L.M. and Zapata, M.** (2006)
- 1075 Photoacclimation in phytoplankton: implications for biomass estimates, pigment functionality
- 1076 and chemotaxonomy. *Mar Biol*, **148**, 963-971. <https://doi.org/10.1007/s00227-005-0138-7>
- 1077 **Rokka, A., Suorsa, M., Saleem, A., Battchikova, N. and Aro, E.M.** (2005) Synthesis and assembly
- 1078 of thylakoid protein complexes: multiple assembly steps of photosystem II. *Biochem J*, **388**,
- 1079 159-168. <https://doi.org/10.1042/Bj20042098>
- 1080 **Rutschow, H., Ytterberg, A.J., Friso, G., Nilsson, R. and van Wijk, K.J.** (2008) Quantitative
- 1081 proteomics of a chloroplast SRP54 sorting mutant and its genetic interactions with CLPC1 in
- 1082 *Arabidopsis*. *Plant Physiol*, **148**, 156-175. <https://doi.org/10.1104/pp.108.124545>
- 1083 **Rütgers, M. and Schroda, M.** (2013) A role of VIPP1 as a dynamic structure within thylakoid
- 1084 centers as sites of photosystem biogenesis. *Plant Signal. Behav.*, **8**, e27037.
- 1085 <https://doi.org/10.4161/psb.27037>
- 1086 **Serôdio, J., Vieira, S., Cruz, S. and Coelho, H.** (2006) Rapid light-response curves of chlorophyll
- 1087 fluorescence in microalgae: relationship to steady-state light curves and non-photochemical
- 1088 quenching in benthic diatom-dominated assemblages. *Photosynth Res*, **90**, 29-43.

- 1089 <https://doi.org/10.1007/s11120-006-9105-5>
- 1090 **Siebenaller, C., Junglas, B. and Schneider, D.** (2019) Functional implications of multiple IM30
1091 oligomeric states. *Front Plant Sci*, **10**. <https://doi.org/10.3389/fpls.2019.01500>
- 1092 **Sundberg, E., Slagter, J.G., Fridborg, I., Cleary, S.P., Robinson, C. and Coupland, G.** (1997)
1093 ALBINO3, an Arabidopsis nuclear gene essential for chloroplast differentiation, encodes a
1094 chloroplast protein that shows homology to proteins present in bacterial membranes and yeast
1095 mitochondria. *Plant Cell*, **9**, 717-730. <https://doi.org/10.1105/tpc.9.5.717>
- 1096 **Suomi, T., Seyednasrollah, F., Jaakkola, M.K., Faux, T. and Elo, L.L.** (2017) ROTS: An R
1097 package for reproducibility-optimized statistical testing. *PLoS Comput Biol*, **13**.
1098 <https://doi.org/10.1371/journal.pcbi.1005562>
- 1099 **Theis, J., Niemeyer, J., Schmollinger, S., Ries, F., Rutgers, M., Gupta, T.K., Sommer, F.,
1100 Muranaka, L.S., Venn, B., Schulz-Raffelt, M., Willmund, F., Engel, B.D. and Schroda,
1101 M.** (2020) VIPP2 interacts with VIPP1 and HSP22E/F at chloroplast membranes and
1102 modulates a retrograde signal for *HSP22E/F* gene expression. *Plant Cell Environ*, **43**, 1212-
1103 1229. <https://doi.org/10.1111/pce.13732>
- 1104 **Theis, J. and Schroda, M.** (2016) Revisiting the photosystem II repair cycle. *Plant Signal Behav*,
1105 **11**, e1218587. <https://doi.org/10.1080/15592324.2016.1218587>
- 1106 **Träger, C., Rosenblad, M.A., Ziehe, D., Garcia-Petit, C., Schrader, L., Kock, K., Richter, C.V.,
1107 Klinkert, B., Narberhaus, F., Herrmann, C., Hofmann, E., Aronsson, H. and
1108 Schunemann, D.** (2012) Evolution from the prokaryotic to the higher plant chloroplast signal
1109 recognition particle: the signal recognition particle RNA is conserved in plastids of a wide
1110 range of photosynthetic organisms. *Plant Cell*, **24**, 4819-4836.
1111 <https://doi.org/10.1105/tpc.112.102996>
- 1112 **Trösch, R., Mühlhaus, T., Schroda, M. and Willmund, F.** (2015) ATP-dependent molecular
1113 chaperones in plastids - More complex than expected. *Bba-Bioenergetics*, **1847**, 872-888.
1114 <https://doi.org/10.1016/j.bbabi.2015.01.002>
- 1115 **Walter, B., Hristou, A., Nowaczyk, M.M. and Schünemann, D.** (2015a) *In vitro* reconstitution of
1116 co-translational D1 insertion reveals a role of the cpSec-Alb3 translocase and Vippl1 in
1117 photosystem II biogenesis. *Biochem J*, **468**, 315-324. <https://doi.org/10.1042/Bj20141425>
- 1118 **Walter, B., Pieta, T. and Schunemann, D.** (2015b) *Arabidopsis thaliana* mutants lacking cpFtsY or
1119 cpSRP54 exhibit different defects in photosystem II repair. *Front Plant Sci*, **6**, 250.
1120 <https://doi.org/10.3389/fpls.2015.00250>
- 1121 **Waterhouse, A., Bertoni, M., Bienert, S., Studer, G., Tauriello, G., Gumienny, R., Heer, F.T.,
1122 de Beer, T.A.P., Rempfer, C., Bordoli, L., Lepore, R. and Schwede, T.** (2018) SWISS-
1123 MODEL: homology modelling of protein structures and complexes. *Nucleic Acids Res*, **46**,
1124 W296-W303. <https://doi.org/10.1093/nar/gky427>
- 1125 **Wickström, D., Wagner, S., Baars, L., Ytterberg, A.J., Klepsch, M., van Wijk, K.J., Luirink, J.
1126 and de Gier, J.W.** (2011) Consequences of depletion of the signal recognition particle in
1127 *Escherichia coli*. *J Biol Chem*, **286**, 4598-4609. <https://doi.org/10.1074/jbc.M109.081935>
- 1128 **Witt, H.T.** (1979) Energy conversion in the functional membrane of photosynthesis. Analysis by
1129 light pulse and electric pulse methods. The central role of the electric field. *Biochim Biophys
1130 Acta*, **505**, 355-427. [https://doi.org/10.1016/0304-4173\(79\)90008-9](https://doi.org/10.1016/0304-4173(79)90008-9)
- 1131 **Wu, H.Y., Cockshutt, A.M., McCarthy, A. and Campbell, D.A.** (2011) Distinctive photosystem
1132 II photoinactivation and protein dynamics in marine diatoms. *Plant Physiol*, **156**, 2184-2195.
1133 <https://doi.org/10.1104/pp.111.178772>
- 1134 **Wu, H.Y., Roy, S., Alami, M., Green, B.R. and Campbell, D.A.** (2012) Photosystem II
1135 photoinactivation, repair, and protection in marine centric diatoms. *Plant Physiol*, **160**, 464-

- 1136 476. <https://doi.org/10.1104/pp.112.203067>
- 1137 **Zhang, D., Sweredoski, M.J., Graham, R.L., Hess, S. and Shan, S.O.** (2012) Novel proteomic
1138 tools reveal essential roles of SRP and importance of proper membrane protein biogenesis.
1139 *Mol Cell Proteomics*, **11**, M111 011585. <https://doi.org/10.1074/mcp.M111.011585>
- 1140 **Ziehe, D., Dunschede, B. and Schunemann, D.** (2017) From bacteria to chloroplasts: evolution of
1141 the chloroplast SRP system. *Biol Chem*, **398**, 653-661. <https://doi.org/10.1515/hsz-2016-0292>
- 1142 **Ziehe, D., Dunschede, B. and Schunemann, D.** (2018) Molecular mechanism of SRP-dependent
1143 light-harvesting protein transport to the thylakoid membrane in plants. *Photosynth Res*, **138**,
1144 303-313. <https://doi.org/10.1007/s11120-018-0544-6>

1145

1146 **Table 1. Growth rates of WT and *cpsrp54* mutant lines acclimated to different light intensities.**
1147 Maximum cell divisions per day during the exponential phase were calculated from three biological
1148 replicates of WT and *cpsrp54* KO lines acclimated to LL (35 $\mu\text{mol photons m}^{-2} \text{s}^{-1}$), ML (200 μmol
1149 $\text{photons m}^{-2} \text{s}^{-1}$) and HL (1000 $\mu\text{mol photons m}^{-2} \text{s}^{-1}$). Values are presented with $\pm\text{SD}$.

1150

1151 **Table 2. Proteomics data.** Proteins encoded in the chloroplast genome or predicted to contain
1152 chloroplast transit peptides sequences that were significantly regulated (FDR <0.01) in the same
1153 direction in both *cpsrp54-8* and *cpsrp54-11* lines compared to WT after 6 h in ML showing \log_2 ratios
1154 $\geq \pm 0.5$ for at least one of the mutant lines and where at least two unique peptides were detected. Only
1155 proteins with a Score sequest HT >10 were included in the table. Ratios were calculated based on
1156 results from five biological replicates for each line. Downregulated proteins are marked in bold. †Low
1157 molecular weight proteins included despite detection of only one unique peptide. The abbreviations
1158 used are: Psa: PSI proteins; Psb: PSII proteins; FNR: ferredoxin NAPD(H) reductase; atp: chloroplast
1159 ATP synthase proteins; LHCX: light-harvesting complex stress-related proteins; APX: Ascorbate
1160 peroxidase; VIPP1: vesicle-inducing protein in plastids 1; ClpB: Caseinolytic proteases of subfamily
1161 B; chlI: Magnesium chelatase I subunit; HEMB: porphobilinogen synthase; rps13: 30S ribosomal
1162 protein S13; sCdc48: SELMA Cell division cycle 48; IPMDH: isopropylmalate dehydrogenase;
1163 FbaC2: Fructose-1,6-bisphosphate aldolase C2

1164

1165 **Table 3. Overview of the effect of loss of CpSRP54 in diatom (*P. tricornutum*), plant (*A. thaliana*)**
1166 **and green algae (*C. reinhardtii*) model organisms.** Symbols and abbreviations used are NC = no
1167 change; ↓ = downregulated compared to WT; ↑ = upregulated compared to WT; n/a = not assessed

1168

1169 **Figure 1. Structural features of diatom CpSRP54 proteins. a)** Schematic view of the conserved
1170 domains of CpSRP54. The area of the CpSRP54 protein corresponding to the 20-bp target region for
1171 CRISPR/Cas9-based gene editing is located in the N-terminal helical bundle domain (N-domain),

1172 with the protospacer adjacent motif (PAM) target site located at the forward DNA strand (green
1173 character). The diatom and *Bolidophytes* native insertion sequence between the G1 and G2 domains
1174 are shown above the figure. CTP: chloroplast-targeting peptide; V: variable domain; N: SRP54 N-
1175 terminal helical bundle domain; G: SRP GTPase containing domain; M: SRP54 signal peptide
1176 binding domain. **b)** Protein alignment showing the insert region between the G1 and G2 domains in
1177 diatoms. **c)** Protein model of diatom CpSRP54 highlighting the insert region (dots) and the docking
1178 site with FTSY. **d)** Protein alignment of the C-terminal region of the M-domain containing the
1179 conserved RR-motif. **e)** Overview of amino acid sequences resulting from CRISPR/Cas9-mediated
1180 indels in the three *cpsrp54* knock out lines, causing premature stop codons and truncated CpSRP54
1181 proteins. The A1 allele in *cpsrp54-20* could not be amplified by PCR and is indicated by “?”. Color
1182 coding is as follows: Wild-type (WT) target sequence: blue characters; altered amino acids as a result
1183 of indels: red characters. Asterisks indicate premature stops.

1184

1185 **Figure 2. Color and spectral properties of WT and *cpsrp54* mutants.** **a)** Culture color of LL-
1186 acclimated WT and *cpsrp54* mutants at equal cell densities. **b)** *In vivo* fluorescence excitation spectra
1187 and **c)** absorbance spectra of cultures acclimated to LL. Fluorescence emission was measured at 730
1188 nm to allow for full visible range (400 – 700 nm) fluorescence excitation. Presented spectra for all
1189 lines are representative of three replicates per line.

1190

1191 **Figure 3. Pigment levels, DES index and NPQ capacity in WT and *cpsrp54* mutant cell lines.**
1192 Cellular pigment contents (fmol/cell) are shown for **a)** Chl *a*, **b)** Fx, **c)** Ddx, and **d)** Dtx in WT and
1193 *cpsrp54* mutant cells as a function of time following a shift from LL conditions (0 h; 35 $\mu\text{mol photons}$
1194 $\text{m}^{-2} \text{s}^{-1}$) to ML conditions (200 $\mu\text{mol photons m}^{-2} \text{s}^{-1}$) for 0.5, 6, 24, 48, and 168 h. **e)** DES index [DES
1195 = $\text{Dtx}/(\text{Dtx} + \text{Ddx})$] calculated from data shown in C and D. **f)** Induction of NPQ as a function of
1196 increasing light intensity was calculated from rapid light curves derived from LL-acclimated cells.
1197 $\text{NPQ} = (F_{m'_{\text{max}}}/F_{m'}) - 1$. $F_{m'_{\text{max}}}$ replaces the commonly used F_m , since $F_{m'}$ values frequently occur at
1198 low light intensities that are higher than the F_m from dark-treated diatom samples (Serôdio *et al.*,
1199 2006). Results are presented as means of three biological replicates \pm SD. Black circles indicate
1200 individual data points for the replicates. Asterisks describe significant differences between *cpsrp54*
1201 mutants and WT as indicated by two-way ANOVA with Dunnet's multiple comparison tests ($p <$
1202 0.05).

1203 **Figure 4. Photophysiological responses of WT and *cpsrp54* mutant cell lines after a shift from**
1204 **LL to ML conditions. a)** Photosynthetic (PSII) efficiency (F_v/F_m), **b)** Maximum light-utilization
1205 coefficient (α), **c)** Photosynthetic capacity ($rETR_{max}$), and **d)** Light saturation index (E_k) in WT and
1206 *cpsrp54* mutant cells as a function of time following a shift from LL conditions (0 h; 35 $\mu\text{mol photons}$
1207 $\text{m}^{-2} \text{s}^{-1}$) to ML conditions (200 $\mu\text{mol photons m}^{-2} \text{s}^{-1}$) for 0.5, 6, 24, 48, and 168 h. **e)** In vivo assessment
1208 of PSII/PSI reaction centers ratios and **f)** Photosynthetic electron flow in LL and ML-acclimated
1209 cultures. Results are presented as means of three biological replicates \pm SD. Black circles indicate
1210 individual data points for the replicates. Asterisks indicate the results of two-way ANOVA with
1211 Dunnet's multiple comparison test ($p < 0.05$)

1212

1213 **Figure 5. Photosynthetic efficiency (F_v/F_m) in WT and *cpsrp54* mutant lines as a response to HL**
1214 **with or without addition of the chloroplast protein synthesis inhibitor lincomycin (LINC).** LL-
1215 acclimated WT and *cpsrp54* lines was treated with or without lincomycin (LINC) before exposure to
1216 60 min of HL (1000 $\mu\text{mol photons m}^{-2} \text{s}^{-1}$) followed by 30 min recovery in dim light. WT data are
1217 presented as averages of three biological replicates \pm SD. *Cpsrp54* data are averages of the three
1218 *cpsrp54* lines 8, 11 and 20, three biological replicates of each line (in total $n = 9$) \pm SD.

1219

1220 **Figure 6. Analysis of thylakoid membrane protein accumulation at different light conditions in**
1221 **WT and *cpsrp54* mutant lines. a)** Abundance of FCP proteins belonging to the LHCF group and
1222 PSII core proteins D1 and D2 in LL-acclimated cells, after 6h in ML and in cells acclimated to ML.
1223 The LHCF antibody is predicted to detect LHCF1-11 (Juhas *et al.*, 2014). An antibody recognizing
1224 the β -subunit of ATP synthase (AtpB) was used as loading control on each of the individual blots.
1225 Images have been cropped. Relative quantification of **b)** LHCF1-11, **c)** D1 and **d)** D2 protein
1226 accumulation in *cpsrp54* lines compared to WT in LL and ML-acclimated cells was performed using
1227 ImageJ to estimate band intensity. All values were normalized against AtpB included as a loading
1228 control on all blots. Ratios presented are an average of results calculated from two independent
1229 experiments and minimum three different blots with 1-3 biological replicates included in each blot.
1230 10 μg total protein was loaded in each well. Black circles indicate individual data points for the
1231 replicates.

1232 **Figure 7. Models of the CpSRP pathway for integration of thylakoid membrane (TM) proteins**
1233 **in *P. tricornutum* compared to plant (*A. thaliana*) and green algae (*C. reinhardtii*) model**
1234 **organisms. a)** Schematic overview of the suggested roles of members of the CpSRP pathway in *P.*
1235 *tricornutum*. CpSRP54, likely in interaction with its receptor CpFTSY, are proposed to guide
1236 translating ribosomes to the ALB3a insertase and possibly the CpSecY translocase for co-
1237 translational insertion of chloroplast encoded TM proteins (right side). FCP proteins synthesized by
1238 ribosomes on the chloroplast endoplasmic reticulum membrane (cERM) are transported through the
1239 four membranes surrounding diatom chloroplasts and eventually delivered to ALB3b in an unknown
1240 manner independent of the CpSRP pathway (left side). **b)** Schematic overview of the roles of
1241 members of the CpSRP pathway in *A. thaliana*. Several members of the CpSRP pathway (CpSRP54,
1242 CpFTSY; ALB3) have dual roles and function in both post-translational insertion of LHCPs (left side)
1243 and co-translational insertion of chloroplast encoded proteins (right side) into the TM membrane.
1244 LTD and CpSRP43 of the post-translational CpSRP pathway are not present in diatom genomes. LTD
1245 delivers LHCPs to the CpSRP43/CpSRP54 complex that in the next step interacts with CpFTSY
1246 before integration of LHCPs into TMs through ALB3. **c)** Schematic overview of the roles of members
1247 of the CpSRP pathway in *C. reinhardtii*. The CpSRP pathway of *C. reinhardtii* comprises mostly the
1248 same key molecular players as *A. thaliana*, but CpSRP54 and CpFTSY are proposed to function
1249 exclusively in the post-translational CpSRP pathway. Here CpSRP54 is not complexed to CpSRP43,
1250 but CpSRP54 is believed to function further downstream. Similar to diatoms, but in contrast to plants,
1251 two different ALB3 insertases function in the post- and co-translational CpSRP pathway.
1252 Abbreviations used are: cERM: chloroplast endoplasmic reticulum membrane; PPM: periplastidial
1253 membrane; OEM: outer envelope membrane; IEM: inner envelope membrane; FCP: Fx-Chl *a/c*-
1254 binding proteins; LHCP: Light harvesting complex proteins; LTD: LHCP translocation defect
1255 protein; Cp: Chloroplast; SRP: signal recognition particle.
1256

1257 **Table 1.**

	35 $\mu\text{mol s}^{-1}\text{m}^{-2}$	200 $\mu\text{mol s}^{-1}\text{m}^{-2}$	1000 $\mu\text{mol s}^{-1}\text{m}^{-2}$
WT	1.54 \pm 0.24	2.23 \pm 0.03	2.03 \pm 0.18
<i>cpsrp54-8</i>	1.41 \pm 0.18	1.61 \pm 0.14	1.55 \pm 0.03
<i>cpsrp54-11</i>	1.38 \pm 0.26	1.75 \pm 0.09	1.46 \pm 0.15
<i>cpsrp54-20</i>	1.38 \pm 0.28	1.77 \pm 0.12	1.60 \pm 0.06

1258

1259

1260

1261

1262

Table 2.

Protein ID	Name	Function (predicted)	Location (predicted)	Nucleus (N)/Chloroplast (C)-encoded	<i>cpsrp54-8</i> /WT (log ₂ ratio)	<i>cpsrp54-11</i> /WT (log ₂ ratio)	# unique peptides	# peptides	Score sequest HT
A0T096	CP43 (PsbC)	PSII core	TM	C	-0.58	-0.44	9	9	51.1
A0T097	D2 (PsbD)	PSII core	TM	C	-2.03	-0.69	2	2	10.85
A0T0G0	PsbY ⁺	PSII core	TM	C	-0.93	-1.31	1	1	14.09
B7G6V4	PsbP	PSII OEC	TM	N	0.39	0.65	4	4	11.02
A0T0C9	PetA	Cytb ₆ f	TM	C	-0.78	-0.47	10	10	63.72
B5Y3C9	PetC2	Cytb ₆ f	TM	N	-0.56	-0.49	5	5	11.94
A0T0L2	PsaC	PSI core	TM	C	-0.34	-0.65	4	4	24.56
A0T0B9	PsaD	PSI core	TM	C	-0.41	-0.73	7	7	24.3
A0T0F3	PsaE ⁺	PSI core	TM	C	-0.71	-0.61	1	1	26.67
A0T0M1	PsaF	PSI core	TM	C	-0.53	-0.56	3	3	49.68
A0T0M6	PsaL	PSI core	TM	C	-0.51	-0.62	2	2	18.61
B7GCT8	FNR	Ferredoxin-NADP reductase	Stroma/TM bound	N	0.80	0.66	8	10	248.79
B7G0M5	FNR	Ferredoxin-NADP reductase	Stroma/TM bound	N	1.34	1.44	4	6	53.69
A0T0F1	atpA	ATP synthase	TM	C	-0.33	-0.63	16	19	178.79
A0T0F0	atpD	ATP synthase	TM	C	-1.12	-0.62	4	4	12.1
B7FYLO	LHCX1	Photoprotection	TM	N	0.35	0.79	4	4	46.83
B7FR60	LHCX2	Photoprotection	TM	N	0.56	0.59	3	3	108.13
B7G386	APX	ROS scavenging	TM-bound	N	0.61	0.64	13	13	101.35
B7FU48	Cyclophilin type peptidyl-prolyl cis-trans isomerase	Formation of PSII	Lumen	N	0.68	0.54	4	4	22.24
B7FWP5	VIPP1	TM biogenesis/ /remodeling, PSII biogenesis	TM surface, stroma	N	0.90	0.76	7	7	30.86
B5Y3P1	DNAJ	Co-chaperone	Stroma	N	0.48	0.55	7	7	27.24
A0T0H7	DnaK	Chaperone	Stroma	C	1.48	1.62	35	35	244.61
B5Y5I5	ClpB	Chaperone	Stroma	N	0.68	0.61	9	9	40.91
B7FVE3	Tic62-NAD(P)-related group II protein	Unknown	Chloroplast	N	0.30	0.71	3	3	10.07
B7FUD8	Tic62-NAD(P)-related group II protein	Unknown	Chloroplast	N	1.06	0.69	4	4	22.86
B7FPG9	Oligopeptidase A	Hydrolysis of peptide bond	Chloroplast	N	0.70	0.55	8	8	51.31
A0T0B5	chlI	Biosynthesis of Chl	Stroma	C	-0.57	-0.57	6	6	12

B7FSN7	AlaD (HemB)	Biosynthesis of Chl	Stroma	N	0.69	0.70	5	5	24.11
A0T0J8	rps13	Translation	Chloroplast	C	-0.65	-0.52	3	3	29.5
B7G1T3		Degradation of chloroplast membrane proteins	Chloroplast membrane-associated	N	-0.53	-0.51	5	6	11.81
B5Y3B2	sCdc48		Chloroplast	N	1.22	0.88	2	2	17.17
	Myo-inositol 2-dehydrogenase	Metabolism		N					
B7G1X8	IPMDH	Amino-acid biosynthesis	Stroma	N	-0.96	-0.80	6	6	27.81
B7G9G9	FbaC2	Carbohydrate metabolism	Stroma	N	0.44	0.71	5	5	35.95

1264

1265

1266

1267

1268

1269

1270

1271

1272

1273

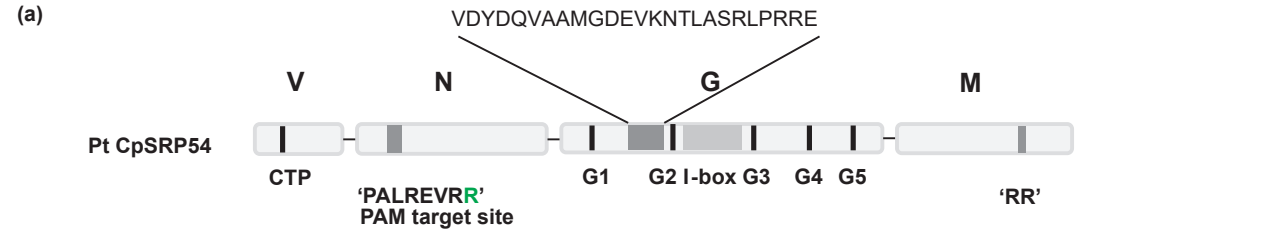
1274

1275

1276

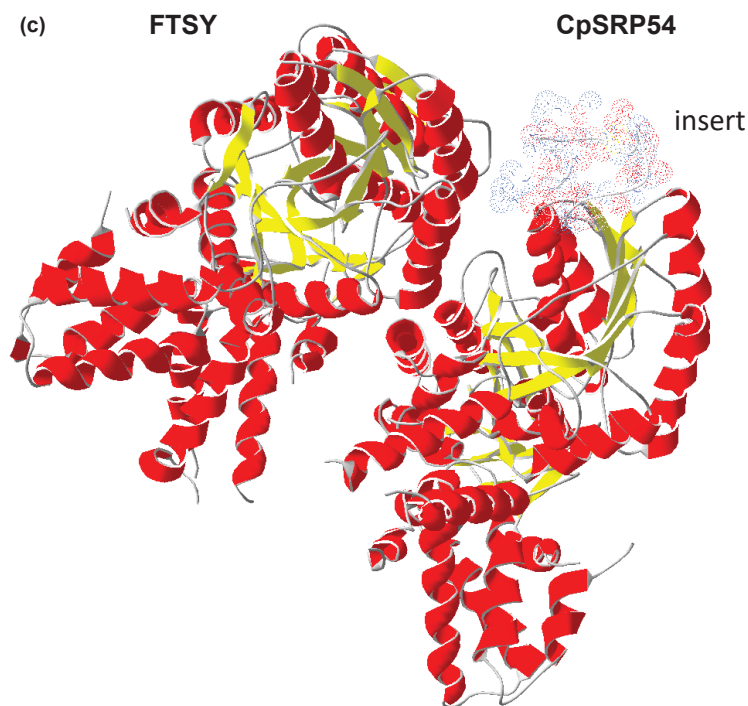
Table 3.

Effects of loss of CpSRP54	<i>P.</i> <i>tricornutum</i>	<i>A.</i> <i>thaliana</i>	<i>C.</i> <i>reinhardtii</i>	<i>References</i>
Color	NC	↓	↓	Present paper; Amin <i>et al.</i> , 1999; Rutschow <i>et al.</i> , 2008; Jeong <i>et al.</i> , 2017
LHC proteins	NC	↓	↓	Present paper; Amin <i>et al.</i> , 1999; Rutschow <i>et al.</i> , 2008; Jeong <i>et al.</i> , 2017
Proteins of photosynthetic complexes	↓	↓	NC	Present paper; Amin <i>et al.</i> , 1999; Rutschow <i>et al.</i> , 2008; Hristou <i>et al.</i> , 2029; Jeong <i>et al.</i> , 2017
Light harvesting pigments	NC	↓	↓	Present paper; Amin <i>et al.</i> , 1999; Jeong <i>et al.</i> , 2017
Photoprotective pigments during light stress	↑	n/a	n/a	Present paper
Chaperones (compensating mechanisms)	↑	↑	n/a	Present paper; Amin <i>et al.</i> , 1999; Rutschow <i>et al.</i> , 2008
Growth in low light intensities	NC	↓	n/a	Present paper; Rutschow <i>et al.</i> , 2008
Growth at higher light intensities	↓	↓	↑	Present paper; Rutschow <i>et al.</i> , 2008; Jeong <i>et al.</i> , 2017
Photosynthetic performance in low light	NC	NC	NC	Present paper; Hutin <i>et al.</i> , 2002; Jeong <i>et al.</i> , 2017
Photosynthetic performance at higher light intensities	↓	↓	NC	Present paper; Hutin <i>et al.</i> , 2002; Jeong <i>et al.</i> , 2017
PSII repair	↓	↓	n/a	Present paper; Walter <i>et al.</i> , 2015



(b)

	G1	insert region	G2	
<i>Phaeodactylum t.</i>	DEAVILLAGLQAGKTTAAGKLALFLKEREVDYDQVAAMGDEVK--NTLASRLPRRE		RKVVLLVAADIVRPAAIKQIQOVLGEGS	251
<i>Fistulifera s.</i>	NEAVILLAGLQAGKTTAAGKLALYLKEREVNYDMVDKDLDSAK--MLASRLPTRN		RVNVLVAADVVRPAAIQIQEILGKS	242
<i>Seminavis r.</i>	KEFVLLAGLQAGKTTAAGKLALYLKEREVDYDAVNPEDDQET--QLASKLPKRR		RKVVLLVAADVVRPAAIKQIEILGEGS	256
<i>Thalassiosira p.</i>	EEAVILLAGLQAGKTTAAGKLALYLQEREVDPPALSSMSDEDRSSTLASRMPKRN		RKVVLLVAADVVRPAAIQIQOILGKS	243
<i>Skeletonema m.</i>	EEAVILLAGLQAGKTTAAGKLALYLKEREVDPNAISELSEERSKTLASRLPKRN		RKVVLLVAADVVRPAAIQIQOILGKQ	259
<i>Bolidomonas sp.</i>	GLITVLLMAGLQAGKTTACAKLAKYLMEDVEVSWEAVDSMPKELSETLSTRLPKSR		RVVLLVACDVRPAAREQIHLVLCGR	255
<i>Nannochloropsis g.</i>	PEFVILLAGLQAGKTTAAAKLALYQCSRAEKAEAF-----		EKILMVAAADVVRPAIDQIQLTGER	219
<i>Chondrus c.</i>	EEFVLLAGLQAGKTTAAAKLALYCLKEE-----		RSVMMVAADVVRPAIDQIKTLGKS	139
<i>Chlamydomonas r.</i>	FEQIILMAGLQGVKTTAAGKLALYLKKA-----		KSCQLLVATDVMRPAIDQIVKLGA	218
<i>Arabidopsis t.</i>	GEFVILLAGLQGVKTTVCAKLACYLKKQG-----		KSCMLVACDVMRPAIDQIVILCEQ	229
<i>Oryza s.</i>	GEFVILLAGLQGVKTTVCAKLAFLYLLKLG-----		KSCMLVAADVVRPAIDQITILCEQ	223
<i>Physcomitrella p.</i>	GEFVILLMAGLQGVKTTACGKLALFCKKKG-----		KSVMMVATDVMRPAIDQIVTLGKQ	278



(d)

	'RR'	
<i>Phaeodactylum t.</i>	GNRAMRISKNK	571
<i>Fistulifera s.</i>	GNRAMRKKTNT	562
<i>Seminavis r.</i>	GNRASRKNKKR	583
<i>Thalassiosira p.</i>	GNRNARIKGKK	476
<i>Skeletonema m.</i>	GNRNARIKGKK	577
<i>Nannochloropsis g.</i>	QNRQARIQSRR	551
<i>Chondrus c.</i>	KNRAQRKKKAL	453
<i>Chlamydomonas r.</i>	APGKVRKEPLS	539
<i>Arabidopsis t.</i>	PPGTARRKRK	545
<i>Oryza s.</i>	PPGTARRKRK	540
<i>Physcomitrella p.</i>	APGTAIRGFAS	594

(e)

WT	76	GPKRRMSEASIQPALREVRALLDADVNVVDVADTLIEGVRARSLGQEVLEG	126
<i>cpsrp54 - 8</i>	A1:	GPKRRMSEASIQPALREVTSGASRRGCQR*	
	A2:	GPKRRMSEASIQPALREVTSGASRRGCQR*	
<i>cpsrp54 - 11</i>	A1:	GPKRRMSEASIQPALREVVSGASRRGCQR*	
	A2:	GPKRRMSEASIQPALREGASRRGCQR*	
<i>cpsrp54 - 20</i>	A1:	?	
	A2:	GPKRRMSEASIQPALREVRSWPARRRPGSSWTRPPTTRRTARPGRAPTR*	

